Geometry II
Discrete Differential Geometry

Alexander I. Bobenko

April 21, 2020

Preliminary version for the summer semester 2020.

Contents

There is no canonical way of defining a discrete surface. We usually think of discrete surfaces as surfaces build from vertices, edges and faces. As an example consider

simplicial surfaces Surfaces glued from triangles.
We see that not every possibility of gluing together triangles constitutes in something we want to call a discrete surface.

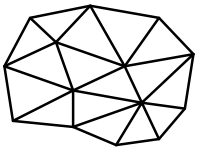

discrete surface

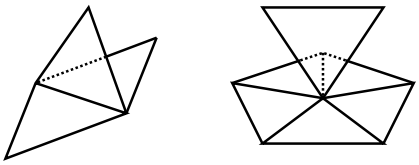

not discrete surfaces

Generalizing the faces to be polygons we obtain the notion of

polyhedral surfaces Surfaces glued from planar polygons.

In particular

simple surfaces Polyhedral surfaces with all vertices of valence three.
They can be seen as an analogue of the characterization of a surface via enveloping tangent planes. Start with a simplicial surface and add a plane at every vertex. By intersecting neighboring planes we obtain another polyhedral surface. Since three planes generically intersect in one point we obtain a vertex for every face of the original surface and a face for each vertex. This means that the obtained surface is combinatorically dual to the simplicial surface. The faces are now planar polygons and all vertices of valence three.

Another special case of polyhedral surfaces are

quad-surfaces Surfaces glued from quadrilaterals
They are analogues of parametrized surfaces. For each quad there is two unique transversal directions given by pairs of opposite edges leading to parameter lines consisting of strips of quadrilaterals.
A reasonable generalization here is to consider non-planar quads.

Dropping the combinatorial structure completely one might consider

point samples Surfaces generated by sets of points. But it is not clear when a set of points without further structure should be considered a discrete surface or how to obtain this additional structure. E.g. In the domain of computer graphics the non-trivial problem of obtaining a water tight polyhedral surface from a "point cloud" is considered.

Reasonable data from an experiment, e.g. scanning a 3D-object could be not only positions but also normal directions. Providing each point with a normal vector or equivalently with a tangent plane leads to

contact elements Points with planes. This can be seen as a notion of a surface together with its Gauss map.

We will mainly deal with polyhedral surfaces and begin by specifying how vertices, edges and faces constitute a discrete surface.

1 Abstract discrete surfaces

We consider discrete surfaces consisting of vertices, edges and faces from the point of view of topology (abstract discrete surfaces), metric geometry (piecewise flat surfaces) and Euclidean geometry (polyhedral surfaces).

1.1 Cell decompositions of surfaces

From the topological point of view a discrete surface is a decomposition of a two-dimensional manifold into vertices, edges and faces. This is what we call the *combinatorics* of a discrete surface.

First some preliminary definitions

Definition 1.1 (surface)**.** A *surface* is a real two-dimensional connected manifold, possibly with boundary.

Remark 1.1. We mainly focus on compact surfaces and compact closed surfaces.

Definition 1.2 (n-cell)**.** We denote the open disk in $\mathbb{R}^n$ by

$$D^n \coloneqq \{x \in \mathbb{R}^n \mid \|x\| < 1\}$$

and its boundary by

$$\partial D^n \coloneqq \overline{D^n} \backslash D^n,$$

where the bar denotes the topological closure.
An *n-dimensional cell* or *n-cell* is a topological space homeomorphic to D^n.

Remark 1.2. Note that $D^0 = \{0\}$ is a point and its boundary $\partial D^0 = \varnothing$.

Definition 1.3 (cell decomposition)**.** Let M be a surface and $T = \{U_i\}_{i=1}^N$ a covering of M by pairwise disjoint 0-, 1- and 2-cells.
T is called a finite *cell decomposition* of M if for any n-cell $U_i \in T$ there is a continuous map

$$\varphi_i : \overline{D^n} \to M$$

which maps D^n homeomorphic to U_i and ∂D^n to a union of cells of dimension at most $n-1$, i.e. 1-cells are bounded by 0-cells and 2-cells by 1- and 0-cells.
0-cells are called *vertices*, 1-cells *edges* and 2-cells *faces*.

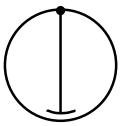

Figure 1.1. This is not a cell decomposition.

Remark 1.3.

- More requirements are needed to define infinite cell decompositions.
- The existence of a finite cell decomposition makes a surface necessarily compact.
- Cell decompositions of surfaces are a special case of *cell complexes*. E.g. a 1-dimensional cell complex is a *graph*.

Example 1.1. A convex polyhedron induces a cell decomposition of $\mathbb{S}^2$.

We introduce some additional properties coming from polyhedra theory but mostly deal with general cell decompositions.

Definition 1.4 (regular and strongly regular)**.** A cell decomposition $T = \{U_i\}_{i=1}^N$ of a surface M is called *regular* if the maps $\varphi_i : \overline{D^n} \to M$ are homeomorphisms.
A regular cell decomposition is called *strongly regular* if for any two cells U_i and U_j the intersection of their closures $\overline{U_i} \cap \overline{U_j}$ is either empty or the closure of *one* cell.

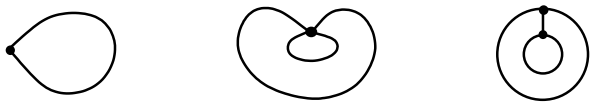

Figure 1.2. Examples of non-regular cell decompositions. Cells with boundary identifications –i.e. self-touching cells– are not allowed. E.g. no loops.

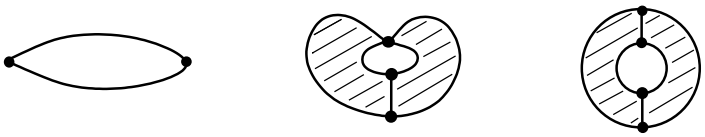

Figure 1.3. Examples of non-strongly regular cell decompositions. Cells with multiple common boundary components are not allowed. E.g. no double edges.

Example 1.2.

(1) The cell decompositions of $\mathbb{S}^2$ induced by convex polyhedra are strongly regular.

(2) Cube with a hole:

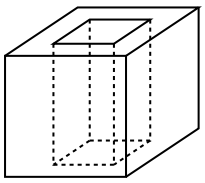

This is not a cell-decomposition of the cube with a hole.

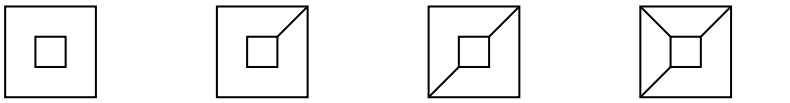

Figure 1.4. Cube with a hole. From "not a cell decomposition" to a strongly regular cell decomposition by adding edges.

Definition 1.5 (abstract discrete surface)**.** Let T be a cell decomposition of a surface M. Then we call the combinatorial data $\mathcal{S} \coloneqq (M, T)$ an *abstract discrete surface* and a homeomorphism $f : M \to \mathbb{R}^n$ its *geometric realization*. We write this as $f : \mathcal{S} \to \mathbb{R}^n$.

Remark 1.4.

- Abstract discrete surfaces are compact.
- We use the terms vertices, edges and faces for the combinatorial cells $U_i \in T$ as well as for the images under the geometric realization $f(U_i) \subset f(M) \subset \mathbb{R}^n$.

Example 1.3 (quad-graph)**.** A *quad-graph* is an abstract discrete surface with all faces being quadrilaterals. A geometric realization with planar faces is called a *Q-net*.

1.2 Topological classification of compact surfaces

We outline the topological classification of compact surfaces. This means that we are interested in topological invariants which uniquely identify a compact surface up to homeomorphisms. A cell decomposition of a surface induces the following topological invariant.

Definition 1.6 (Euler characteristic)**.** Let V, E, F be the sets of vertices, edges and faces of an abstract discrete surface $\mathcal{S} \coloneqq (M, T)$ and $|V|$, $|E|$, $|F|$ their cardinalities. Then

$$\chi(M) \coloneqq |V| - |E| + |F|$$

is called the *Euler characteristic* of M.

Remark 1.5. Since the Euler characteristic is independent of the cell decomposition T of M and every compact surface has a cell decomposition[1], this indeed defines a topological invariant of the surface M.

Example 1.4.

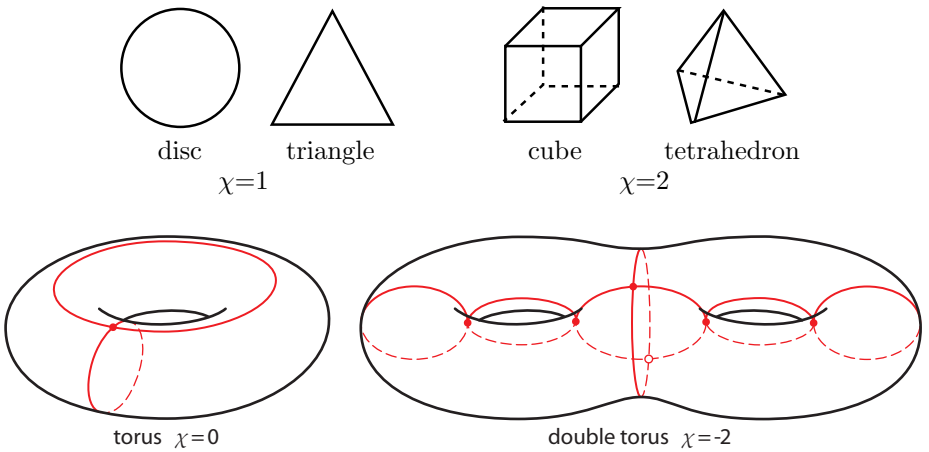

Figure 1.5. Cell decompositions of a disk, sphere, torus and double torus. With Euler characteristic $\chi = |V| - |E| + |F|$.

We describe the construction of closed surfaces by combining some elementary compact closed surfaces of high Euler characteristic using the connected sum. The classification theorem then states that this already yields all possible compact closed surfaces up to homeomorphisms.

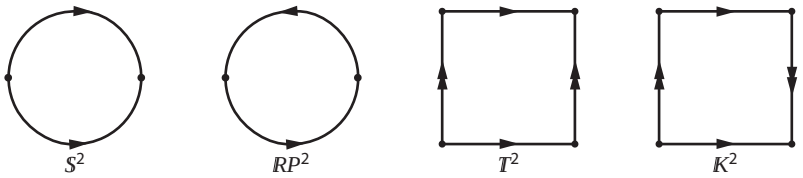

Figure 1.6. Elementary closed surfaces from identifying edges of bigons and quadrilaterals.

There are two essentially different ways of orienting the two edges of a bigon. Identifying the two edges along these orientations yields the *sphere* $\mathbb{S}^2$ and the *real projective plane* $\mathbb{R}\mathrm{P}^2$ respectively. The first of which is orientable while the second is not. Counting vertices, edges and faces of the cell decompositions induced by the original bigon we obtain the Euler characteristics

$$\chi(\mathbb{S}^2) = 2 - 1 + 1 = 2, \quad \chi(\mathbb{R}\mathrm{P}^2) = 1 - 1 + 1 = 1.$$

Pairwise identifying the four edges of a quadrilateral gives us two additional

[1] Even stronger: Every compact surface has a triangulation.
Note that abstract discrete surfaces –which is our case of interest– are compact and always come with a cell decomposition.

surfaces which are the *torus* $\mathbb{T}^2$ and the *Klein bottle* $\mathbb{K}^2$ with

$$\chi(\mathbb{T}^2) = 1 - 2 + 1 = 0, \quad \chi(\mathbb{K}^2) = 1 - 2 + 1 = 0.$$

We notice that the torus and the Klein bottle can not be distinguished by their Euler characteristic alone. But the torus is orientable while the Klein bottle is not.

For two surfaces M and N their connected sum $M\#N$ is obtained by removing an open disk from each and gluing the resulting surfaces together along the circular boundary components of the missing disks.
This operation is associative, commutative and the sphere is the identity element, i.e.

$$M\#\mathbb{S}^2 = \mathbb{S}^2\#M = M$$

Let us determine the Euler characteristic of the connected sum $M\#N$. Consider a cell decomposition of M and N respectively. A cell decomposition of M° which is the surface M with an open disk removed can be obtained by adding one edge as a loop at one vertex of the cell decomposition of M, so

$$\chi(M^\circ) = \chi(M) - 1.$$

Same for N°. Gluing along the circular boundaries is then equivalent to the identification of these new edges and the adjacent vertex. So we have one edge less and one vertex less in the connected sum which cancel out in the Euler characteristic

$$\chi(M\#N) = \chi(M^\circ) + \chi(N^\circ) - 1 + 1 = \chi(M) + \chi(N) - 2.$$

Starting with a sphere as the identity element we construct surfaces of lower Euler characteristic by connecting tori, projective planes and Klein bottles to it. Connecting g tori to the sphere[2] yields an orientable surface with g holes, i.e.

$$\chi((\mathbb{T}^2)^{\#g}) = \chi(\mathbb{T}^2\#\ldots\#\mathbb{T}^2) = 2 - 2g, \qquad g \geqslant 0,$$

where we define $M^{\#0} \coloneqq \mathbb{S}^2$ by the identity element. g is called the *genus* of the resulting surface.

Building the connected sum of h projective planes we obtain surfaces of odd and even Euler characteristic all of them non-orientable.[3]

$$\chi((\mathbb{RP}^2)^{\#h}) = \chi(\mathbb{RP}^2\#\ldots\#\mathbb{RP}^2) = 2 - h, \qquad h \geqslant 1.$$

Any other combination of connected sums of our elementary surfaces $\mathbb{S}^2$, $\mathbb{T}^2$, $\mathbb{RP}^2$ and $\mathbb{K}^2$ does not yield new surfaces. Indeed building the connected sum of two projective planes already gives us a Klein bottle

$$\mathbb{RP}^2\#\mathbb{RP}^2 = \mathbb{K}.$$

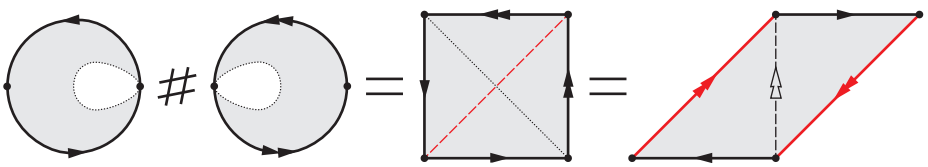

Figure 1.7. The connected sum of two projective planes is a Klein bottle.

[2] Or equivalently to each other.
[3] Any connected sum containing at least one projective plane is non-orientable.

Attaching another projective plane to the Klein bottle is the same as attaching it to a torus[4]

$$\mathbb{K}\#\mathbb{R}\mathrm{P}^2 = \mathbb{T}^2\#\mathbb{R}\mathrm{P}^2.$$

So any mixed combinations of tori and projective planes are already included.[5]

$\mathbb{T}^2$ and $\mathbb{R}\mathrm{P}^2$ together with the connected sum $\#$ generate a monoid of which the classification theorem states that it already includes all compact closed surfaces.

Theorem 1.1 (classification by connected sums)**.** *Any compact closed surface M is either homeomorphic to the connected sum of $g \geqslant 0$ tori*

$$M = (\mathbb{T}^2)^{\#g}$$

or to the connected sum of $h \geqslant 1$ real projective planes

$$M = (\mathbb{R}\mathrm{P}^2)^{\#h}.$$

In the first case M is orientable and in the second non-orientable.

And as an immediate consequence of our considerations about the Euler characteristics

Corollary 1.2 (classification by orientability and Euler characteristic)**.** *Any compact closed surface is uniquely determined by its orientability and Euler characteristic up to homeomorphisms.*

Remark 1.6.

- A compact closed orientable surface can be classified by its Euler characteristic only, or equivalently by its genus g since

$$\chi(M) = 2 - 2g.$$

- The classification theorem can be generalized to compact surfaces with boundary by adding another topological invariant which is the number of connected boundary components k. In this case the Euler characteristic for orientable surfaces becomes

$$\chi(M) = 2 - 2g - k.$$

- The easiest and most recent proof of the classification theorem is Conway's ZIP proof which can be found in [FW99].

- The procedure of identifying edges of bigons and quadrilaterals to obtain compact closed surfaces can be generalized to the pairwise identification of edges of even-sided polygons. This leads to other possible ways of classification.

[4] We see that the connected sum has no inverse operation.

[5] This can be restated more general in the following way. On any non-orientable surface there is no way to distinguish a handle from an attached Klein-bottle.

2 Polyhedral surfaces and piecewise flat surfaces

We start with a short presentation of curvature in the classical smooth theory.

2.1 Curvature of smooth surfaces

Extrinsic curvatures of a smooth surface immersed in $\mathbb{R}^3$ are defined as follows. Consider the one parameter family of tangent spheres $S(\kappa)$ with signed curvature κ touching the surface at a point p. κ is positive if the sphere lies at the same side of the tangent plane as the normal vector and negative otherwise. Let M be the set of tangent spheres intersecting any neighborhood U of p in more than one point. The values

$$\kappa_1 \coloneqq \inf_{S\in M} \kappa(S), \quad \kappa_2 \coloneqq \sup_{S\in M} \kappa(S)$$

are called the *principal curvatures* of the surface at p.

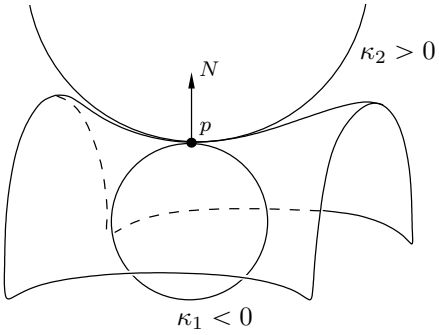

Figure 2.1. The curvature spheres touching the surface in p.

The spheres $S(\kappa_1)$ and $S(\kappa_2)$ are called *principal curvature spheres* and are in second order contact with the surface. The contact directions are called *principal directions* and are orthogonal.

The *Gaussian curvature* and *mean curvature* are defined as

$$K \coloneqq \kappa_1\kappa_2, \quad H \coloneqq \frac{1}{2}\left(\kappa_1 + \kappa_2\right).$$

The Gaussian curvature of a surface at a point p is also the quotient of oriented areas $A(\cdot)$:

$$K(p) = \lim_{\varepsilon\to 0} \frac{A\left(N\left(U_\varepsilon(p)\right)\right)}{A\left(U_\varepsilon(p)\right)},$$

where $U_\varepsilon(p)$ is an ε-neighborhood of p on the surface, and $N(U_\varepsilon(p)) \subset S^2$ is its image under the Gauss map.
The following classical theorems hold.

Theorem 2.1 (Gauss' Theorema Egregium)**.** *The Gaussian curvature of a surface is preserved by isometries.*

Theorem 2.2 (Gauss-Bonnet)**.** *The total Gaussian curvature of a compact closed surface S is given by*

$$\int_S K \mathrm{d}A = 2\pi\chi(S).$$

2.1.1 Steiner's formula

The *normal shift* of a smooth surface S with normal map N is defined as

$$S_\rho := S + \rho N.$$

For sufficiently small ρ the surface S_ρ is also smooth. Interpreting S as an enveloping surface of the principal sphere congruences one can show that the centers of the principal curvature spheres of S and S_ρ coincide. The signed radii are reduced by ρ so the principal curvatures change as

$$\frac{1}{\kappa_{1\rho}} = \frac{1}{\kappa_1} - \rho, \quad \frac{1}{\kappa_{2\rho}} = \frac{1}{\kappa_2} - \rho.$$

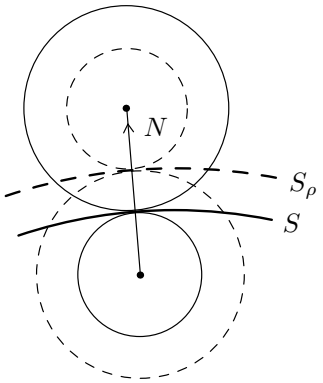

Theorem 2.3 (Steiner's formula)**.** *Let S be a smooth surface and S_ρ its smooth normal shift for sufficiently small ρ. Then the area of S_ρ is a quadratic polynomial in ρ,*

$$A(S_\rho) = A(S) - 2H(S)\rho + K(S)\rho^2,$$

where $K(S) = \int_S K \mathrm{d}A$ and $H(S) = \int_S H \mathrm{d}A$ are the total Gaussian and total mean curvature of S.

Proof. Let $\mathrm{d}A$ and $\mathrm{d}A_\rho$ be the area forms of S and S_ρ. The normal shift preserves the Gauss map, therefore one has

$$K\mathrm{d}A = K_\rho \mathrm{d}A_\rho,$$

where K and K_ρ are the corresponding Gaussian curvatures. For the area this implies

$$\begin{aligned} A(S_\rho) &= \int_{S_\rho} \mathrm{d}A_\rho = \int_S \frac{K}{K_\rho}\mathrm{d}A \\ &= \int_S \kappa_1\kappa_2(\frac{1}{\kappa_1} - \rho)(\frac{1}{\kappa_2} - \rho)\mathrm{d}A \\ &= \int_S \left(1 - (\kappa_1 + \kappa_2)\rho + \kappa_1\kappa_2\rho^2\right)\mathrm{d}A \\ &= A(S) - 2H(S)\rho + K(S)\rho^2. \end{aligned} \tag{2.1}$$

□

Remark 2.1. Equation (2.1) also holds true without integration. We can state Steiner's formula in the differential version

$$\mathrm{d}A_\rho = (1 - 2H(p)\rho + K(p)\rho^2)\mathrm{d}A,$$

where $K(p)$ and $H(p)$ are the (local) Gaussian and mean curvature at p.

2.2 Curvature of polyhedral surfaces

Definition 2.1 (polyhedral surface)**.** A *polyhedral surface* in $\mathbb{R}^n$ is a geometric realization $f : \mathcal{S} \to \mathbb{R}^n$ of an abstract discrete surface $\mathcal{S} = (M, T)$ such that the edges are intervals of straight lines and the faces are planar.
A *simplicial surface* is a polyhedral surface with all faces being triangles.

2.2.1 Discrete Gaussian curvature

For a polyhedral surface the Gaussian curvature is concentrated at vertices in the following sense: The area of $N(U_\varepsilon(p))$ vanishes for all internal points on faces and edges. For a vertex it is equal to the oriented area of the corresponding spherical polygon.

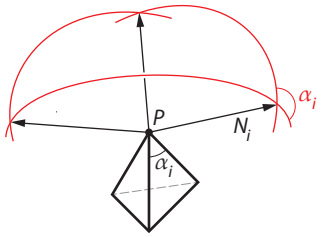

Figure 2.2. The angle α_i at vertex p is the external angle of the spherical polygon at vertex N_i.

Let N_i be the normal vectors of the faces adjacent to the vertex p. Each two neighboring normals define a geodesic line on $\mathbb{S}^2$, which all together constitute a spherical polygon. The angle α_i at vertex p of the face on the polyhedral surface with normal vector N_i is equal to the external angle of the spherical polygon at the vertex N_i. So the angle defect $2\pi - \sum \alpha_i$ at the vertex p is the area of the spherical polygon where $\sum \alpha_i$ is the total angle on the polyhedral surface around the vertex p.[6]

Definition 2.2 (discrete Gaussian curvature)**.** For a closed polyhedral surface S the angle defect

$$K(p) := 2\pi - \sum_i \alpha_i \tag{2.2}$$

at a vertex p is called the *Gaussian curvature* of S at p.
The *total Gaussian curvature* is defined as the sum

$$K(S) := \sum_{p \in V} K(p).$$

The points with $K(p) > 0$, $K(p) = 0$ and $K(p) < 0$ are called *elliptic*, *flat* and *hyperbolic* respectively.

[6] This is an oriented area since the "external angle" depends on the orientation of the polygon.

Remark 2.2. The angle defect at a vertex p is bounded from above by 2π but unbounded from below.

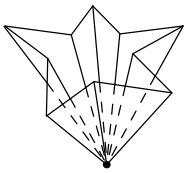

Figure 2.3. The discrete Gaussian curvature at a vertex p can be made arbitrarily low by "folding" a vertex star.

Lemma 2.4. *Let p be an inner point of a polyhedral surface. Then*

$$\begin{aligned} p \text{ convex} &\Rightarrow p \text{ elliptic} \\ p \text{ planar} &\Rightarrow p \text{ flat} \\ p \text{ saddle} &\Rightarrow p \text{ hyperbolic}, \end{aligned}$$

where

$$\begin{aligned} p \text{ convex} &:\Leftrightarrow \text{the spherical polygon of the normal vectors around } p \text{ is convex} \\ p \text{ planar} &:\Leftrightarrow p \text{ and its neighbors lie in a plane} \\ p \text{ saddle} &:\Leftrightarrow p \text{ lies in the convex hull of its neighbors (and } p \text{ not planar).} \end{aligned}$$

Remark 2.3. In general, none of the implications in Lemma 2.4 is reversible.

Since the discrete Gaussian curvature is defined intrinsically[7] we immediately obtain a discrete version of Gauss' Theorema Egregium.

Theorem 2.5 (polyhedral Gauss' Theorema Egregium)**.** *The Gaussian curvature of a polyhedral surface is preserved by isometries, i.e. depends on the polyhedral metric only.*

There also holds a discrete version of the Gauss-Bonnet theorem.

Theorem 2.6 (polyhedral Gauss-Bonnet)**.** *The total Gaussian curvature of a closed polyhedral surface S is given by*

$$K(S) = 2\pi\chi(S).$$

Proof. We have

$$K(S) = \sum_{p \in V} K(p) = 2\pi\,|V| - \sum_{\text{all angles of } S} \alpha_i.$$

The angles $\pi - \alpha_i$ are the (oriented) external angles of a polygon. Their sum is

$$\sum_{\substack{\text{all angles of} \\ \text{one polygon}}} (\pi - \alpha_i) = 2\pi.$$

[7] The cone angle $\sum \alpha_i$ is invariant under isometries. We discuss this and polyhedral metrics in more detail in Section 2.3.

The sum over all faces gives

$$2\pi\,|F| = \sum_{\text{all angles of } S} (\pi - \alpha_i) = 2\pi|E| - \sum_{\text{all angles of } S} \alpha_i,$$

where we used that the number of angles is equal to $2|E|$ (each edge is associated with 4 attached angles but each angle comes with two edges).
Finally

$$K(S) = 2\pi(|V| - |E| + |F|) = 2\pi\chi(S).$$

□

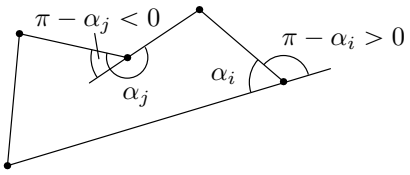

Figure 2.4. Oriented external angles of a polygon.

Example 2.1 (Gaussian curvature of a cube)**.** Consider a standard cube with all vertex angles equal to $\frac{\pi}{2}$. Then the Gaussian curvature at every vertex p is

$$K(p) = 2\pi - 3\frac{\pi}{2} = \frac{\pi}{2}.$$

So the sum over all eight vertices yields $K(S) = 4\pi$.
On the other hand $\chi(S) = \chi(\mathbb{S}^2) = 2$.

Remark 2.4. The polyhedral Gauss-Bonnet theorem can be extended to polyhedral surfaces with boundary. Since the boundary components of a polyhedral surface are piecewise geodesic we only have to add the turning angle of the boundary curve

$$\varphi(p) \coloneqq \pi - \sum_i \alpha_i$$

at each boundary vertex p to the total discrete Gaussian curvature.[8]

2.2.2 Discrete mean curvature

Definition 2.3 (discrete mean curvature)**.** The *discrete mean curvature* of a closed polyhedral surface S at the edge $e \in E$ is defined by

$$H(e) := \frac{1}{2}\theta(e)l(e),$$

where $l(e)$ is the length of e, and $\theta(e)$ is the oriented angle between the normals of the adjacent faces sharing the edge e (the angle is considered to be positive in the convex case and negative otherwise).
The *total mean curvature* is defined as the sum over all edges

$$H(S) := \sum_{e\in E} H(e) = \frac{1}{2}\sum_{e\in E} \theta(e)l(e).$$

[8] Or alternatively define the discrete Gaussian curvature at boundary vertices by the turning angle.

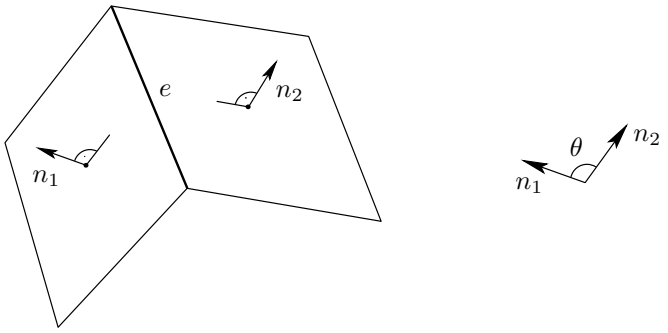

Figure 2.5. Discrete mean curvature for polyhedral surfaces.

With this definition the following discrete version of Steiner's formula holds true.

Theorem 2.7 (Steiner's formula for convex polyhedra)**.** *Let $\mathcal{P}$ be a convex polyhedron with boundary surface $S = \partial\mathcal{P}$. Let $\mathcal{P}_\rho$ be the parallel body at the distance ρ*

$$\mathcal{P}_\rho := \left\{ p \in \mathbb{R}^3 \mid d(p, \mathcal{P}) \leqslant \rho \right\}.$$

Then the area of the boundary surface $S_\rho := \partial\mathcal{P}_\rho$ is given by

$$A(S_\rho) = A(S) + 2H(S)\rho + 4\pi\rho^2. \tag{2.3}$$

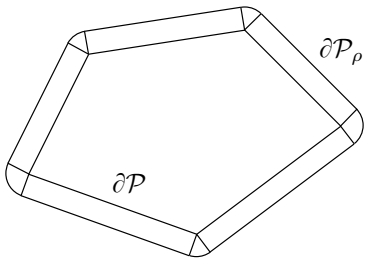

Figure 2.6. Boundary surface S of a convex polyhedron and S_ρ of its parallel body at distance ρ.

Proof. The parallel surface S_ρ consists of three parts:

- Plane pieces congruent to the faces of S.
  Their areas sum up to $A(S)$.
- Cylindrical pieces of radius ρ, angle $\theta(e)$ and length $l(e)$ along the edges e of S with area $\theta(e)l(e)\rho = 2H(e)\rho$.
- Spherical pieces at the vertices p of S with area $K(p)\rho^2$. Since a convex polyhedron is a topological sphere the Gaussian curvature sums up to $K(S) = 4\pi$, i.e. merged together by parallel translation the spherical pieces comprise a round sphere of radius ρ.

□

Remark 2.5 (Steiner's formula for polyhedral surfaces). At non-convex edges and vertices we can define the parallel surface as depicted in Figure 2.7

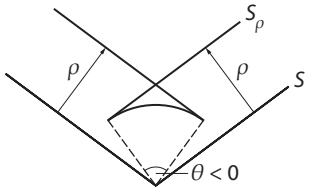

Figure 2.7. On the definition of the parallel surface S_ρ in the non-convex case.

and take the area of the corresponding cylindrical and spherical pieces as negative. Then Steiner's formula for an arbitrary closed polyhedral surface S reads as follows:

$$A(S_\rho) = A(S) + 2H(S)\rho + K(S)\rho^2,$$

where $K(S) = 2\pi\chi(S)$ is the total Gaussian curvature.

2.3 Polyhedral Metrics

We want to investigate the intrinsic geometry induced by polyhedral surfaces.

Definition 2.4. A *metric* on a set M is a map

$$d : M \times M \to \mathbb{R}$$

such that for any $x, y, z \in M$

(i) $d(x, y) \geqslant 0$

(ii) $d(x, y) = 0 \Leftrightarrow x = y$

(iii) $d(x, y) = d(y, x)$

(iv) $d(x, y) + d(y, z) \geqslant d(x, z)$

The pair (M, d) is called a *metric space*.
Let (M, d) and $(\tilde{M}, \tilde{d})$ be two metric spaces. Then a map $f : M \to \tilde{M}$ such that for any $x, y \in M$

$$\tilde{d}(f(x), f(y)) = d(x, y)$$

is called an *isometry*.
(M, d) and $(\tilde{M}, \tilde{d})$ are called *isometric* if there exists a bijective isometry $f : M \to \tilde{M}$ called a *global isometry*.
(M, d) is called *locally isometric* to $(\tilde{M}, \tilde{d})$ at a point $x \in M$ if there exists a neighborhood U of x and a neighborhood $\tilde{U} \subset \tilde{M}$ such that (U, d) is isometric to $(\tilde{U}, \tilde{d})$.

Remark 2.6.

- Every isometry is continuous and every global isometry a homeomorphism.
- An abstract discrete surface $\mathcal{S} = (M, T)$ equipped with a metric becomes a *metric space* (M, d).
- For a geometric realization $f : \mathcal{S} \to \mathbb{R}^n$ the Euclidean metric on $\mathbb{R}^n$ induces a metric on $f(M) \subset \mathbb{R}^n$. To study this metric intrinsically on the corresponding abstract discrete surface $\mathcal{S}$ we pull it back, i.e. we define the metric on $\mathcal{S}$ such that f is an isometry.

Let $f : \mathcal{S} \to \mathbb{R}^n$ be a polyhedral surface. We examine the metric induced by the Euclidean metric of $\mathbb{R}^n$. For two points $x, y \in f(M)$ we are interested in the length $L(\gamma)$ of the shortest curve γ lying on $f(M)$ connecting x and y:

$$d(x, y) = \inf_{\gamma} \{L(\gamma) \mid \gamma : [0, 1] \to f(M), \gamma(0) = x, \gamma(1) = y\} .$$

Example 2.2 (shortest paths on a polyhedral surface)**.** Isometrically unfolding a cube to a plane we see that connecting two points by a straight line might not always constitute a shortest path.

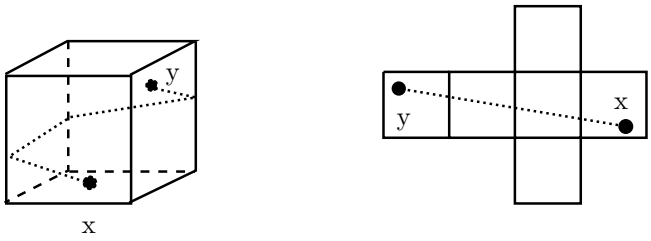

Figure 2.8. Straight line on a cube which is not the shortest path connecting x and y.

Shortest paths are a global property of the metric.

We start by investigating locally shortest paths which are called geodesics. We look for local isometries to some planar domain where we already know the geodesics.

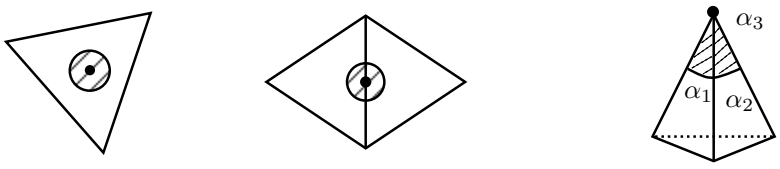

Figure 2.9. Neighborhoods of a point on a face, edge and vertex of a polyhedral surface.

Consider a point $p \in M$ on a face $A \in F$. Then a small enough neighborhood of $f(p)$ on $f(M)$ is entirely contained in the planar face $f(A)$. So the neighborhood can be mapped isometrically to a disk D^2.

For points on edges a small neighborhood intersects the interior of two planar faces. Isometrically unfolding those two faces to a plane we find that the neighborhood is also isometric to a disk.
For points on a vertex we could also unfold the adjacent faces to a plane. But this leaves a cut in the neighborhood. What we can do isometrically is map the small neighborhood to the tip of a cone characterized by the angle θ which is the sum of angles α_i between the edges adjacent to the vertex. The *angle defect*

$$K(p) \coloneqq 2\pi - \theta$$

is a measure for the non-flatness of the metric at p.
In general θ can be greater than 2π in which case the cone becomes a saddle. We make the following classification

$K > 0$ elliptic point, locally isometric to a cone.

$K = 0$ flat point, locally isometric to a disk,
i.e. the vertex and its adjacent edges could be completely removed from the combinatorics without changing the polyhedral surface.

$K < 0$ hyperbolic point, locally isometric to a saddle.

We find that the metric induced on the polyhedral surface $f(M)$ by the Euclidean metric in $\mathbb{R}^n$ is locally equivalent to the Euclidean metric of $\mathbb{R}^2$ everywhere except for the vertices.

Pulling back the metric with the map f to the abstract discrete surface $\mathcal{S}$ we obtain a metric with the same properties, i.e. a small neighborhood of a point $p \in M$ on a

- face is isometric to a disk D^2.
- edge is isometric to a disk D^2.
- vertex is isometric to the tip of a cone.

We can now forget about the combinatorics and obtain an abstract surface M with a polyhedral metric which we call piecewise flat surface.

Definition 2.5 (piecewise flat surface)**.** A metric d on a surface M is called a *polyhedral metric* if (M, d) is locally isometric to a cone at finitely many points $V = \{P_1, \dots, P_N\} \subset M$ (*conical singularities* of the metric) and locally isometric to a plane elsewhere.
The pair (M, d) of a surface and a polyhedral metric is called a *piecewise flat surface*.

Remark 2.7. A polyhedral metric d on a surface M carries no obvious information about edges and faces, only about the vertices.

How to prescribe a polyhedral metric?

We investigate how the information about the metric gets transferred from a polyhedral surface to its corresponding piecewise flat surface (w.l.o.g. we consider simplicial surfaces).
A simplicial surface induces a piecewise flat surface (M, d) together with a triangulation T such that the vertex set includes the conical singularities and all edges are geodesics on (M, d).

Definition 2.6 (geodesic triangulation)**.** Let (M, d) be a piecewise flat surface with conical singularities V_0.
Then a *geodesic triangulation* of (M, d) is a triangulation of M such that its vertex set includes the conical singularities $V_0 \subset V$ and all edges are geodesics on (M, d).

Remark 2.8. In general a geodesic triangulation on a piecewise flat surface does not have to come from a polyhedral surface.

The geodesic triangulation fixes the polyhedral metric of the piecewise flat surface. Its triangles are isometric to Euclidean triangles with straight edges and the polyhedral metric is determined by the lengths of the edges.
The Euclidean triangles on the other hand are uniquely determined by the lengths of its edges if and only if these satisfy the triangle-inequality.
We obtain the following general construction on how to prescribe a polyhedral metric.[9]

- Start with an abstract discrete surface $\mathcal{S} = (M, T)$ where T is a triangulation.
- Define a length function $l : E \to \mathbb{R}_+$ on the edges E of T such that on every face the triangle-inequality is satisfied.

From this data we can construct unique Euclidean triangles which fit together along corresponding edges of T. We can always glue the obtained Euclidean triangles together along the edges around one common vertex –thus obtaining a polyhedral metric on the abstract surface $\mathcal{S}$– but we cannot be sure that they will fit together to constitute a whole polyhedral surface. Summing up the angles at corresponding vertices we obtain the angle defect of the conical singularities of the polyhedral metric.

We get closer to the answer of the questions:

> Is a piecewise flat surface always realizable as a polyhedral surface?
> And is the corresponding polyhedral surface uniquely determined?

Isometric deformations of a simplicial surface preserve its polyhedral metric and therefore the corresponding piecewise flat surface.

Example 2.3 (pushing a vertex in)**.** If all neighbors of a vertex p are coplanar we can reflect the whole vertex star in this plane without changing any angles.

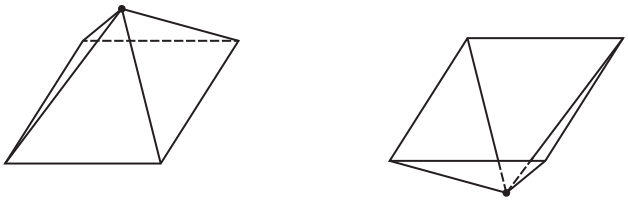

Figure 2.10. Pushing a vertex in does not change the metric.

We obtain the same piecewise flat surface with the same geodesic triangulation. So the polyhedral surface generating a piecewise flat surface is in general not unique.

[9]Note that choosing a triangulation of M –i.e. gluing M together from triangles– to prescribe the polyhedral metric is still eminent in this construction.

Example 2.4 (isometric bending of a polyhedral quadrilateral and edge flipping)**.** Consider two planar triangles with a common edge. Isometrically unfolding the two triangles along the common edge we obtain a planar quadrilateral. If the quadrilateral is convex we can replace the edge by the other diagonal and fold the quadrilateral along this new edge.

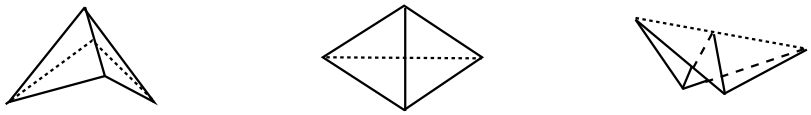

Figure 2.11. Edge flip. Isometrically unfold a quadrilateral to a plane and fold it along the other diagonal.

The edge flip can be done directly on the polyhedral surface without any folding by introducing a non-straight edge.
We obtain a different geodesic triangulation on the same piecewise flat surface which does not necessarily come from a polyhedral surface anymore.

Lemma 2.8 (Possibility of an edge-flip)**.** *Let (M, d) be a piecewise flat surface with a geodesic triangulation T.*
Then an edge e of T can be flipped if its two neighboring triangles are distinct and unfolding them into a plane yields a convex quadrilateral.

Remark 2.9. Since we admit non-regular triangulations we need the condition of the two triangles to be distinct to make the edge flip combinatorially possible.

Example 2.5 (tetrahedron)**.** Four congruent equilateral triangles can be glued together to obtain a tetrahedron.

Figure 2.12. Two geodesic triangulations of the piecewise flat surface given by a tetrahedron.

An edge-flip of one of their edges constitute four triangles which do not fit together as a whole polyhedral surface with the given combinatorics.

We have seen that not every geodesic triangulation of a piecewise flat surface is realizable as a polyhedral surface. Nor is the polyhedral surface we seek uniquely determined even if we know the combinatorics.

We finish this section by stating two classical theorems.

Theorem 2.9 (Burago-Zalgaller, 1960)**.** *Every piecewise flat surface can be realized as a polyhedral surface embedded in* $\mathbb{R}^3$*.*

Remark 2.10*.*

- Note that the ambient space can always be taken to be $\mathbb{R}^3$.
- This is a pure existence statement and the proof gives no indication on how to construct the polyhedral surface.

For convex polyhedral metrics the corresponding polyhedral surface which is convex is unique and can be obtained via a construction algorithm.

Theorem 2.10 (Alexandrov)**.** *Let* (M, d) *be a piecewise flat sphere with a convex polyhedral metric* d*. Then there exists a convex polytope* $\mathcal{P} \subset \mathbb{R}^3$ *such that the boundary of* $\mathcal{P}$ *is isometric to* (M, d)*. Besides,* $\mathcal{P}$ *is unique up to a rigid motion.*

Remark 2.11*.*

- A polyhedral metric d with conical singularities $P_1, \ldots, P_N$ is called convex if all its conical singularities are elliptic, i.e. $K(P_i) \geqslant 0$.
- The edges of $\mathcal{P}$ are a complicated functions of d, since the metric does not distinguish points on edges from points on faces.
- For a proof of this theorem with a construction algorithm see [BI08].
- An implementation of the algorithm can be found at [Sec].

3 Discrete cotan Laplace operator

We introduce a discrete Laplace operator naturally induced by a simplicial surface (or more general by a geodesic triangulation of a piecewise flat surface).

3.1 Smooth Laplace operator in $\mathbb{R}^N$

Let $\Omega \subset \mathbb{R}^N$ be an open set with boundary $\partial\Omega$. We denote the coordinates in $\mathbb{R}^N$ by $x = (x_1, ..., x_N)$. The Laplace operator of a function $f : \Omega \to \mathbb{R}$ is defined by

$$\Delta f = \sum_{i=1}^{N} \frac{\partial^2 f}{\partial x_i^2}$$

A function with $\Delta f = 0$ is called *harmonic*.
The problem of finding a harmonic function with prescribed boundary data $g : \partial\Omega \to \mathbb{R}$

$$\Delta f|_\Omega = 0, \quad f|_{\partial\Omega} = g \tag{DBVP}$$

is known as the *Dirichlet boundary value problem*.
The *Dirichlet energy* is given by

$$E(f) = \frac{1}{2} \int_\Omega |\nabla f|^2 \, \mathrm{d}A,$$

where ∇f is the gradient of f.
Let $\varphi \in \mathcal{C}_0^1(\Omega)$ be a continuously differentiable function with compact support on Ω. Then due to Green's formula

$$\frac{d}{dt} E(f + t\varphi)|_{t=0} = \int_\Omega \langle \nabla f, \nabla \varphi \rangle \mathrm{d}A = \int_\Omega \varphi(\Delta f) \mathrm{d}A.$$

This integral vanishes for arbitrary φ if and only if f is harmonic. So harmonic functions are the critical points of the Dirichlet energy.
For sufficient smooth boundary[10] one can prove the existence and uniqueness of solutions of the Dirichlet boundary value problem (DBVP) for arbitrary continuous $g \in \mathcal{C}(\partial\Omega)$. This solution minimizes the Dirichlet energy.

Remark 3.1. Sometimes the Laplace operator is defined with minus sign to obtain a positive definite operator.

[10] For example of Hölder class $\partial\Omega \in \mathcal{C}^{1+a}$, with some $a > 0$.

3.2 Laplace operator on graphs

Definition 3.1 (Laplace operator and Dirichlet energy on graphs)**.** Let $G = (V, E)$ be a finite graph with vertices V and edges E. Let $\nu : E \to \mathbb{R}$ be a *weight function* defined on the edges of G.
Then the *discrete Laplace operator* on G with weights ν is defined by

$$(\Delta f)(i) = \sum_{j:(ij)=e\in E} \nu(e)(f(i) - f(j))$$

for all $i \in V$ and all functions $f : V \to \mathbb{R}$ on vertices.
The *Dirichlet energy* of f is defined by

$$E(f) = \frac{1}{2} \sum_{(ij)=e\in E} \nu(e)(f(i) - f(j))^2.$$

A function $f : V \to \mathbb{R}$ satisfying $\Delta f = 0$ is called *discrete harmonic*.

Example 3.1. By setting $\nu(e) = 1$ for all $e \in E$ one obtains the *combinatorial Laplace operator*

$$(\Delta f)(i) = \sum_{j:(ij)\in E} (f(i) - f(j))$$

on any graph G.
In the case $G = \mathbb{Z}$ we obtain

$$(\Delta f)(n) = 2f(n) - f(n + 1) - f(n - 1),$$

and for $G = \mathbb{Z}^2$

$$(\Delta f)(n, m) = 4f(m, n) - f(m - 1, n) - f(m + 1, n) - f(m, n - 1) - f(m, n + 1).$$

Let $V_0 \subset V$ (treated as the "boundary" of G).

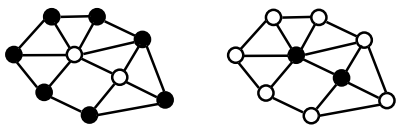

Figure 3.1. The set V_0 of "boundary" vertices on a graph (black vertices in the figure) is arbitrary.

Given some $c : V_0 \to \mathbb{R}$ consider the space of functions with prescribed values on the boundary

$$\mathcal{F}_{V_0,c} = \left\{ f : V \to \mathbb{R} \mid \ f|_{V_0} = c|_{V_0} \right\}.$$

This is an affine space over the vector space $\mathcal{F}_{V_0,0}$.

Theorem 3.1. *A function $f : V \to \mathbb{R}$ is a critical point of the Dirichlet energy $E(f)$ on $\mathcal{F}_{V_0,c}$ if and only if it is harmonic on $V \backslash V_0$, i.e.*

$$\Delta f(i) = 0 \quad \forall i \in V \backslash V_0.$$

Proof. Consider a variation $f + t\varphi \in \mathcal{F}_{V_0,c}$ of $f \in \mathcal{F}_{V_0,c}$, i.e. $\varphi \in \mathcal{F}_{V_0,0}$. We have

$$\begin{aligned} E(f + t\varphi) &= E(f) + t^2 E(\varphi) + t \sum_{(ij)\in E} \nu(ij)(f(i) - f(j))(\varphi(i) - \varphi(j)) \\ &= E(f) + t^2 E(\varphi) + t \sum_{i \in V} \varphi(i) \sum_{j:(ij)\in E} \nu(ij)(f(i) - f(j)) \\ &= E(f) + t^2 E(\varphi) + t \sum_{i \in V} \varphi(i)(\Delta f)(i). \end{aligned}$$

So

$$\left.\frac{\mathrm{d}}{\mathrm{d}t}\right|_{t=0} E(f + t\varphi) = \sum_{i \in V} \varphi(i)(\Delta f)(i) \tag{3.1}$$

vanishes for all $\varphi \in \mathcal{F}_{V_0,0}$ if and only if $\Delta f(i) = 0$ for all $i \in V \backslash V_0$. □

Remark 3.2. We can also state (3.1) in terms of the gradient of the Dirichlet energy as

$$\nabla E(f) = \Delta f \tag{3.2}$$

in the sense that $\partial_{f(i)} E(f) = (\Delta f)(i)$ for all $i \in V$.

If all the weights are positive $\nu : E \to \mathbb{R}_+$ then the discrete harmonic functions have properties familiar from the smooth case.

Theorem 3.2 (maximum principle)**.** *Let $G = (V, E)$ be a connected graph and $V_0 \subset V$. Let Δ be a discrete Laplace operator on G with positive weights. Then a function $f : V \to \mathbb{R}$ which is harmonic on $V \backslash V_0$ can not attain its maximum (and minimum) on $V \backslash V_0$.*

Proof. At a local maximum $i \in V \subset V_0$ of f one has $\Delta f(i) = \sum_{j:(ij)\in E} \nu(ij)(f(i) - f(j)) > 0$, therefore f cannot be harmonic. □

For $V_0 = \varnothing$ this implies:

Corollary 3.3 (discrete Liouville theorem)**.** *A harmonic function on a connected graph with positive weights is constant.*

and for $V_0 \neq \varnothing$:

Corollary 3.4 (dDBVP, uniqueness)**.** *The solution of the discrete Dirichlet boundary value problem with positive weights*

$$\Delta f|_{V \backslash V_0} = 0, \quad f|_{V_0} = c \tag{dDBVP}$$

is unique.

Proof. Let $f, \tilde{f}$ be two solutions of (dDBVP). Then $\varphi \coloneqq \tilde{f} - f \in \mathcal{F}_{V_0,0}$ for which the maximum principle implies $\varphi|_V = 0$. □

Theorem 3.5. *Let $G = (E, V)$ be a finite connected graph with positive weights $\nu : E \to \mathbb{R}_+$ and $\varnothing \neq V_0 \subset V$. Given some $c : V_0 \to \mathbb{R}$ there exists a unique minimum $f : V \to \mathbb{R}$ of the Dirichlet energy on $\mathcal{F}_{V_0,c}$.*
This minimum is the unique solution of the discrete Dirichlet boundary value problem (dDBVP).

Proof. The Dirichlet energy is a function on $\mathcal{F}_{V_0,c} \cong \mathbb{R}^{|V\setminus V_0|}$. We investigate its behavior for $\left\| f|_{V\setminus V_0} \right\| \to \infty$. Define

$$\nu_0 := \min_E \{\nu(e)\}, \quad c_0 := \max_{i\in V_0} \{c(i)\}.$$

For $R > c_0$ let $f(k) > R$ at some vertex $k \in V\setminus V_0$. Let $\gamma_k \subset E$ be a path connecting k to some vertex in V_0. It has at most $|E|$ edges. For the Dirichlet energy this gives the following rough estimate:[11]

$$\begin{aligned} E(f) &\geqslant \frac{1}{2}\nu_0 \sum_{(ij)\in\gamma_k} (f(i) - f(j))^2 \\ &\geqslant \frac{1}{2}\nu_0 \frac{(R - c_0)}{|E|} \to \infty \quad (R \to \infty). \end{aligned}$$

Thus the minimum of the Dirichlet energy is attained on a compact set $\{f \in \mathcal{F}_{V_0,c} \mid |f(i)| < R \ \forall i\}$ with some $R \in \mathbb{R}$.
The uniqueness has already been shown in Corollary 3.4. □

Summarizing we have the following equivalent statements:

- $f \in \mathcal{F}_{V_0,c}$ harmonic, i.e. $\Delta f|_{V\setminus V_0} = 0$, $f|_{V_0} = c$.
- f is a critical point of the Dirichlet energy on $\mathcal{F}_{V_0,c}$, i.e. $\nabla_f E = 0$.
- f is the unique minimum of the Dirichlet energy E on $\mathcal{F}_{V_0,c}$.

[11] Where we use $\sum_{i=1}^n a_i^2 \geqslant \frac{1}{n}\left(\sum_{i=1}^n a_i\right)^2$.

3.3 Dirichlet energy of piecewise affine functions

A discrete function $f : V \to \mathbb{R}$ defined at the vertices of a simplicial surface S uniquely extends to a piecewise affine function $f : S \to \mathbb{R}$.

Theorem 3.6. *Let S be a simplicial surface and $f : S \to \mathbb{R}$ a continuous and piecewise affine function (affine on each face of S).*
Then its (continuous) Dirichlet energy is

$$E(f) = \frac{1}{2}\int_S |\nabla f| \, \dot{A} = \frac{1}{2}\sum_{(ij)\in E} \nu(ij)(f(i) - f(j))^2,$$

with weights

$$\nu(ij) = \begin{cases} \frac{1}{2}\ (\cot\alpha_{ij} + \cot\alpha_{ji}) & \textit{for internal edges} \\ \frac{1}{2}\ \cot\alpha_{ij} & \textit{for external edges} \end{cases} \tag{3.3}$$

called cotan-weights.

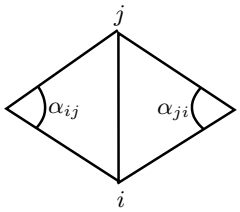

Figure 3.2. α_{ij} and α_{ji} are the angles opposite the edge (ij).

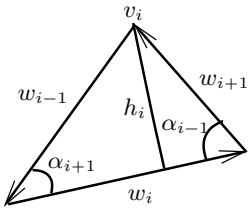

Figure 3.3. Triangle F with vertices v_i, sides a_i, angles α_i and heights h_i.

Proof. We compute the Dirichlet energy of an affine function on a triangle. Denote by $v_1, v_2, v_3 \in \mathbb{R}^N$ the vertices of a triangle F and by $\varphi_1, \varphi_2, \varphi_3$ the basis of affine functions on F given by

$$\varphi_j(i) = \delta_{ij}, \quad i, j = 1, 2, 3.$$

Then $\varphi_1 + \varphi_2 + \varphi_3 = 1$ and an affine function $f : F \to \mathbb{R}$ on the triangle F is determined by its values $f_i = f(v_i)$ at the vertices:

$$f = \sum_{i=1}^{3} f_i \varphi_i.$$

For the gradient of f we obtain

$$|\nabla f|^2 = \left|\sum_{i=1}^{3} f_i^2 \nabla\varphi_i\right|^2 = \sum_{i=1}^{3} f_i \,|\nabla\varphi_i|^2 + 2\sum_{i=1}^{3} f_i f_{i+1}\langle\nabla\varphi_i, \nabla\varphi_{i+1}\rangle, \tag{3.4}$$

where the indices are considered modulo 3.
Denote by α_i the interior angle at vertex v_i, by $w_i \coloneqq v_{i-1} - v_{i+1}$ the directed edge opposite v_i, by $a_i \coloneqq |w_i|$ its lengths, and by h_i the height based at w_i. Then the area of the triangle is given by $A(F) = \frac{1}{2} h_i a_i$, and for the gradient $\nabla\varphi_i$ we obtain

$$\begin{aligned} |\nabla\varphi_i|^2 &= \frac{1}{h_i^2} = \frac{1}{2A(F)}\frac{a_i}{h_i} = \frac{1}{2A(F)}(\cot\alpha_{i-1} + \cot\alpha_{i+1}), \\ \langle\nabla\varphi_i, \nabla\varphi_{i+1}\rangle &= \frac{\langle w_i, w_{i+1}\rangle}{4A(F)^2} = \frac{a_i a_{i+1}\cos\alpha_{i-1}}{4A(F)^2} = -\frac{\cot\alpha_{i-1}}{2A(F)}, \end{aligned}$$

For the gradient (3.4) of f this implies

$$|\nabla f|^2 = \frac{1}{2A(F)}\sum_{i=1}^{3}(f_{i+1} - f_{i-1})^2 \cot\alpha_i.$$

Multiplying by $\frac{1}{2}A(F)$ we obtain the Dirichlet energy of f on F:

$$E(f) = \frac{1}{2}\int_F |\nabla f|^2 \,\mathrm{d}A = \frac{1}{4}\sum_{i=1}^{3}(f_{i+1} - f_{i-1})^2 \cot\alpha_i.$$

□

For a discrete function $f : V \to \mathbb{R}$ defined at the vertices of a geodesic triangulation of a piecewise flat surface (M, d) we can unfold each triangle to the Euclidean plane and define its Dirichlet energy by the affine extension to this triangle in the same way. We also define the corresponding discrete Laplace operator on triangulated piecewise flat surfaces.

Definition 3.2 (discrete Dirichlet energy and discrete cotan Laplace operator)**.** Let (M, d) be a piecewise flat surface, $V \subset M$ a finite set of points that contains all conical singularities. Let $T \in \mathcal{T}_{M,V}$ be a geodesic triangulation of M.
Then we define the *discrete Dirichlet energy* corresponding to T of a function $f : V \to \mathbb{R}$ by

$$E(f) = \frac{1}{2}\sum_{(ij)\in E} \nu(ij)(f(i) - f(j))^2,$$

and the *discrete cotan Laplace operator* corresponding to T by

$$(\Delta f)(i) \coloneqq \sum_{j:(ij)\in E} \nu(ij)(f(i) - f(j))$$

for all $i \in V$ and all functions $f : V \to \mathbb{R}$, with cotan-weights as defined in (3.3).

Remark 3.3.

- The basic relation between the discrete cotan-Laplace operator and the discrete Dirichlet energy is given by (3.1) or (3.2).

- The contan-weights (3.3) are not necessarily positive, and the maximum principle (Theorem 3.2) does not apply for general triangulations. Nonetheless, the discrete Dirichlet energy with cotan-weights is always positive definite, and solutions to (dDBVP) are unique.

3.4 Simplicial minimal surfaces (I)

Consider the area of a triangle in dependence of its edge-lengths:

Lemma 3.7. *Let $a_1, a_2, a_3 > 0$ which satisfy all triangle inequalities $a_i < a_j + a_k$ for $i \neq j \neq k$. Let $A(a_1, a_2, a_3)$ be the area of the Euclidean triangles with edge-lengths a_1, a_2, a_3, and α_i the interior angle opposite a_i, $i = 1, 2, 3$. Then*

$$A(a_1, a_2, a_3) = \frac{1}{4}\left(a_1^2 \cot \alpha_1 + a_2^2 \cot \alpha_2 + a_3^2 \cot \alpha_3\right) \tag{3.5}$$

and

$$\frac{\partial A}{\partial a_i} = \frac{1}{2} a_i \cot \alpha_i \tag{3.6}$$

for $i = 1, 2, 3$.

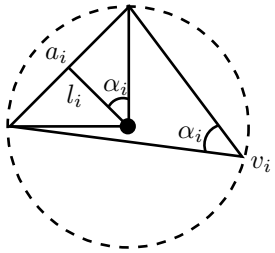

Figure 3.4. Subdivision of a triangle by connecting the center of the circumcircle to its vertices.

Proof. Subdivide the triangle by connecting the center of the circumcircle to its vertices and denote the heights of the three sub-triangles with respect to the base a_i by l_i, $i = 1, 2, 3$ (compare Figure 3.4). Then the area of the sub-triangles is given by

$$\frac{1}{4} a_i l_i = \frac{1}{4} a_i^2 \cot \alpha_i, \qquad i = 1, 2, 3,$$

which sum up to (3.5). Note that l_i, and therefore the corresponding area of the sub-triangle, can be negative. This is the case, if the circumcenter is not contained in the original triangle.

To obtain (3.6) we compute

$$\frac{\partial A}{\partial a_i} = \frac{1}{2} a_i \cot \alpha_i + \frac{1}{4} \sum_{j=1}^{3} a_j^2 \frac{\partial \cot \alpha_j}{\partial a_i},$$

and find that the second term of the right-hand side vanishes:

$$\frac{1}{4} \sum_{j=1}^{3} a_j^2 \frac{\partial \cot \alpha_j}{\partial a_i} = -\frac{1}{4} \sum_{j=1}^{3} \frac{a_j^2}{\sin^2 \alpha_j} \frac{\partial \alpha_j}{\partial a_j} = -R^2 \sum_{j=1}^{3} \frac{\partial \alpha_j}{\partial a_i} = 0,$$

where R is the radius of the circumcircle and $\sum_{j=1}^{3} \frac{\partial \alpha_j}{\partial a_j} = \frac{\partial}{\partial a_j} \sum_{j=1}^{3} \alpha_j = 0$. □

Consider the area of a triangle in dependence of the position of its vertices:

Lemma 3.8. *Let $A(v_1, v_2, v_3)$ be the area of the triangle given by its vertices $v_1, v_2, v_3 \in \mathbb{R}^N$, and denote by α_i the interior angle at v_i, $i = 1, 2, 3$. Then*

$$A(v_1, v_2, v_3) = \frac{1}{4}\left(|v_3 - v_2|^2 \cot\alpha_1 + |v_1 - v_3|^2 \cot\alpha_2 + |v_2 - v_1|^2 \cot\alpha_3\right) \tag{3.7}$$

and

$$\nabla_{v_i} A(v_1, v_2, v_3) = \frac{1}{2}\cot\alpha_j\ (v_i - v_k) + \frac{1}{2}\cot\alpha_k\ (v_i - v_j) \tag{3.8}$$

for $i \neq j \neq k$.

Proof. The length of the edge opposite v_i is given by $a_i := |v_{i-1} - v_{i+1}|$ and (3.7) follows immediately from (3.5).

Differentiating (3.5) we obtain

$$\nabla_{v_i} A = \frac{\partial A}{\partial a_j}\nabla_{v_i} a_j + \frac{\partial A}{\partial a_k}\nabla_{v_i} a_k.$$

Using $\nabla_{v_i} a_j = \nabla_{v_i} |v_i - v_k| = \frac{v_i - v_k}{|v_i - v_k|} = \frac{v_i - v_k}{a_j}$ and (3.6) we obtain (3.8). □

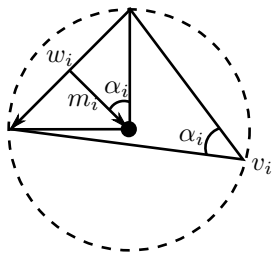

Figure 3.5. Triangle with directed edge w_i and altitude vector m_i of the sub-triangle.

Direct proof of (3.8). We denote by $w_i := v_{i-1} - v_{i+1}$ the directed edges of the triangle, and by m_i the altitude vectors of the three sub-triangles with respect to the base w_i, $i = 1, 2, 3$ (compare Figure 3.5). To obtain the gradient of the area with respect to, say, v_1 we note that the area of the triangle is given by $A = \frac{1}{2}|w_1|\, h_1$ where h_1 is the height based on w_1. Thus, its gradient is

$$\nabla_{v_1} A(v_1, v_2, v_3) = \frac{1}{2} J w_1 \tag{3.9}$$

where J denotes the $\frac{\pi}{2}$-rotation in the plane of the triangle with orientation given by the directed edges. Now for the right-hand side of (3.9) we obtain

$$\begin{aligned}\frac{1}{2}Jw_1 &= -\frac{1}{2}J(w_2 + w_3) = -J(m_2 - m_3) = \frac{|m_2|}{|w_2|}w_2 - \frac{|m_3|}{|w_3|}w_3 \\ &= \frac{1}{2}\cot\alpha_2\ w_2 - \frac{1}{2}\cot\alpha_3\ w_3.\end{aligned}$$

□

Now we can represent the area of a simplicial surface as a Dirichlet energy:

Theorem 3.9. *Let $f : \mathcal{S} \to \mathbb{R}^N$, $S \coloneqq f(\mathcal{S})$ be a simplicial surface, where $f : V \to \mathbb{R}^N$ also denotes its vertices. Let ν be the cotan-weights as defined in (3.3) and $E(f_k)$ the Dirichlet energy of the k-th coordinate function. Then the total area of S is given by*

$$A(S) = 2\sum_{k=1}^{N} E(f_k) = \sum_{(ij)\in E} \nu(ij)\,|f(i) - f(j)|^2 \tag{3.10}$$

where $|f(i) - f(j)|^2 = \sum_{k=1}^{N} |f_k(i) - f_k(j)|^2$ is the square of the edge lengths.

The area gradient at the vertex $f(i)$ is equal to the discrete cotan Laplace operator of f at i:

$$\nabla_{f(i)} A(S) = 2(\Delta f)(i) = 2\sum_{j:(ij)\in E} \nu(ij)(f(i) - f(j)). \tag{3.11}$$

Proof. From (3.7) we find

$$\begin{aligned} A(S) &= \frac{1}{4}\sum_{(ijk)\in F} A(f(i), f(j), f(k)) = \frac{1}{2}\sum_{(ij)\in E} \cot\alpha_{ij}\,|f(i) - f(j)| \\ &= \sum_{k=1}^{N}\sum_{(ij)\in E} \nu(ij)\,|f_k(i) - f_k(j)|^2 \end{aligned}$$

From (3.8) we obtain for the area gradient

$$\nabla_{f(i)} A(S) = \sum_{(ijk)\sim i} \nabla_{f(i)} A(v_i, v_j, v_k) = \sum_{(ij)\sim i} \cot\alpha_{ij}(f(i) - f(j)).$$

□

Remark 3.4.

- For $u : V \to \mathbb{R}^N$ the discrete Laplace operator is understood to act componentwise, e.g.
$$\Delta u = 0 \;\Leftrightarrow\; \Delta u_k = 0\ \forall k = 1, \ldots, N.$$
- We have shown that the gradient at a vertex is given by
$$\nabla_{f(i)} \sum_{k=1}^{N} E(f_k) = (\Delta f)(i),$$
which resembles (3.2) with an $\mathbb{R}^N$-valued f.

  We have used the exact same definition of discrete Dirichlet energy and discrete cotan-Laplace operator as introduced in Section 3.3, but here the cotan-Laplace operator acts on the same function f that determines the weights ν. Thus variations of the simplicial surface f also change the weights, which is the reason why Theorem 3.9 does not immediately follow from (3.2).

We have

$$f \text{ harmonic (w.r.t. cotan Laplace)} \Leftrightarrow S \text{ critical for the area functional.}$$

So we might define *simplicial minimal surfaces* as suggested in [PP93] by

$$S \text{ discrete minimal surface } :\Leftrightarrow \Delta f = 0,$$

which immediately suggests a computation algorithm.

Data: Simplicial surface $f : \mathcal{S} \to S \subset \mathbb{R}^N$
Result: Simplicial minimal surface (w.r.t. cotan Laplace operator).
while *S is not critical for the area functional* **do**
  Compute $\tilde{f}$ such that
  $$\Delta \tilde{f} = 0$$
  which defines a new simplicial surface $\tilde{S}$;
  Replace S by the new surface $\tilde{S}$;
end

Figure 3.6. Simplicial minimal surface algorithm (with cotan Laplace operator).

Remark 3.5. In each step the weights of the discrete contan-Laplace operator are fixed by the simplicial surface f, and we compute a new simplicial surface by the condition $\Delta \tilde{f} = 0$. This is a discrete Dirichlet boundary value problem (dDBVP), and using the discrete Dirichlet energy with cotan-weights the solution is unique if it exists (compare 3.3). The new surface $\tilde{f}$ then carries a new cotan Laplace operator, which is used in the next step.

The weights ν of the discrete cotan Laplace operator can be negative. So it lacks the following property which is a reformulation of the maximum principle for $\mathbb{R}^N$-valued functions.

Proposition 3.10 (local maximum principle)**.** *Let Δ be a discrete Laplace operator on a graph G with positive weights. Let $u : V \to \mathbb{R}^N$ be a map which is harmonic at a vertex $i \in V$.*
Then the value $u(i)$ at the vertex i lies in the convex hull of the values of its neighbors.

Proof. With

$$C \coloneqq \sum_{j:(ij)\in E} \nu(ij)$$

we have

$$(\Delta f)(i) = \sum_{j:(ij)\in E} \nu(ij)\,(f(i) - f(j)) = 0$$
$$\Leftrightarrow\ f(i) = \sum_{j:(ij)\in E} \frac{\nu(ij)}{C} f(j).$$

□

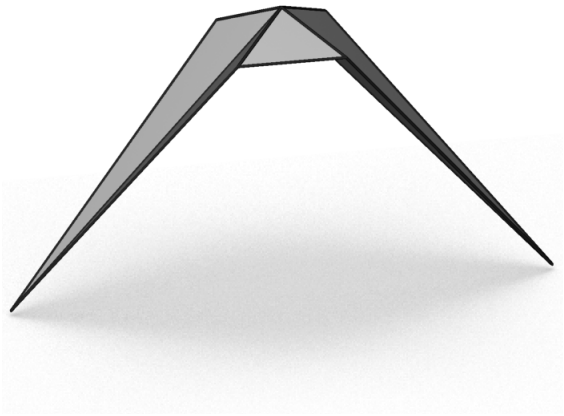

Figure 3.7. Simplicial minimal surface violating the maximum principle. One vertex does not lie in the convex hull of its neighbors.

The maximum principle is a desirable feature analogous to the smooth property of all points of a minimal surface being hyperbolic. So we ask the question

When does the cotan Laplace operator have positive weights?

For an edge $(ij) \in E$ we have

$$\begin{aligned} \nu(ij) &= \frac{1}{2}(\cot \alpha_{ij} + \cot \alpha_{ji}) \\ &= \frac{1}{2}\left(\frac{\cos \alpha_{ij} \sin \alpha_{ji} + \cos \alpha_{ji} \sin \alpha_{ij}}{\sin \alpha_{ij} \sin \alpha_{ji}}\right) \\ &= \frac{\sin(\alpha_{ij} + \alpha_{ji})}{\sin \alpha_{ij} \sin \alpha_{ji}} \geqslant 0 \;\Leftrightarrow\; \alpha_{ij} + \alpha_{ji} \leqslant \pi, \end{aligned} \tag{3.12}$$

which is not satisfied for the long edges in Figure 3.7. We will come back to this when introducing the discrete Laplace-Beltrami operator.

4 Delaunay tessellations

We have noted that the polyhedral metric of a piecewise flat surface (M, d) carries no obvious information about edges and faces. In the following we show how to use the metric to obtain a distinguished geodesic tessellation of (M, d). After recalling the notion of Delaunay tessellations of the plane we demonstrate how to generalize it to piecewise flat surfaces.

4.1 Delaunay tessellations of the plane

4.1.1 Delaunay tessellations from Voronoi tessellations

Consider n distinct points in the plane $V = \{P_1, \dots, P_n\} \subset \mathbb{R}^2$. For each $P_i \in V$ one defines the *Voronoi region*

$$W_{P_i} \coloneqq \left\{P \in \mathbb{R}^2 \mid |PP_i| < |PP_j| \ \forall j \neq i\right\}.$$

With $H_{ij} \coloneqq \left\{P \in \mathbb{R}^2 \mid |PP_i| < |PP_j|\right\}$ we have $W_{P_i} = \bigcap_{j \neq i} H_{ij}$. Thus Voronoi regions are convex polygons.

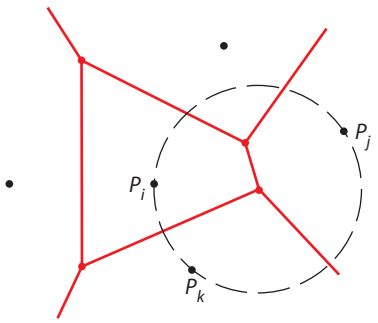

Figure 4.1. Voronoi tessellation for some given points $V = \{P_1, \dots, P_n\}$ in the plane. A vertex Q of the Voronoi tessellation has equal shortest distance to at least three points of V.

Voronoi regions are the 2-cells of the *Voronoi tessellation*.[12]
For $P \in \mathbb{R}^2$ consider

$$\Gamma_{P,V} \coloneqq \left\{P_j \in V \mid |PP_j| = \min_{P_k \in V} |PP_k|\right\}.$$

We can identify points of 2-cells, 1-cells and 0-cells of the Voronoi tessellation by counting points in V that have equal shortest distance to P.
The 2-cells of the Voronoi tessellation are the connected components of

$$\left\{P \in \mathbb{R}^2 \mid \#\Gamma_{P,V} = 1\right\},$$

the 1-cells are the connected components of

$$\left\{P \in \mathbb{R}^2 \mid \#\Gamma_{P,V} = 2\right\},$$

[12] A tessellation is a cell-decomposition with polygonal 2-cells.

and the 0-cells are the points in

$$\left\{P \in \mathbb{R}^2 \mid \#\Gamma_{P,V} \geqslant 3\right\}.$$

For $P' \in \mathbb{R}^2$ with $\#\Gamma_{P',V} = 2$, $P_i, P_j \in \Gamma_{P',V}$, $P_i \neq P_j$ the corresponding 1-cell is given by

$$\left\{P \in \mathbb{R}^2 \mid |PP_i| = |PP_j| < |PP_k| \ \forall k \neq i,j\right\},$$

and for $P \in \mathbb{R}^2$ with $\#\Gamma_P \geqslant 3$, $P_i, P_j, P_k \in \Gamma_{P,V}$ different, the corresponding 0-cell is given by

$$\left\{P \in \mathbb{R}^2 \mid |PP_i| = |PP_j| = |PP_k| \leqslant |PP_m| \ \forall m\right\}.$$

Let Q be a vertex of the Voronoi tessellation, i.e.

$$\exists i,j,k \ \forall m: \ r_Q \coloneqq |PP_i| = |PP_j| = |PP_k| \leqslant |PP_m|.$$

Define the disk

$$D_Q \coloneqq \left\{P \in \mathbb{R}^2 \mid |PQ| < r_Q\right\}.$$

It contains no points of V. But its closure $\bar{D}_Q$ contains at least three. Thus

$$H_Q \coloneqq \operatorname{conv}\left\{P_i \in V \mid |QP_i| = r_Q\right\}$$

is a convex circular polygon.

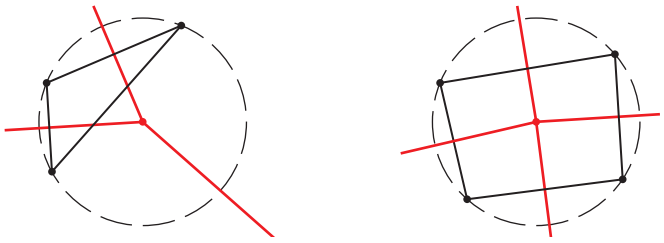

Figure 4.2. Delaunay cells are convex circular polygons. They are triangles in the generic case.

The H_Q are the 2-cells of the *Delaunay tessellation*.
The vertices of this tessellation are V and the edges (P_iP_j) where i,j are indices of neighboring Voronoi cells, i.e. there exists a corresponding Voronoi edge.

Remark 4.1.

- Voronoi and Delaunay tessellations are dual cell-decompositions.
- Corresponding edges of the Voronoi and Delaunay tessellation are orthogonal but do not necessarily intersect (see Figure 4.2). The Voronoi edge bisects the corresponding Delaunay edge.
- Voronoi and Delaunay tessellations of the plane are strongly regular.

- One can also introduce a Delaunay-Voronoi quad-tessellation as a composition of both:

Figure 4.3. Voronoi-Delaunay quad tessellation. Faces (dotted lines) are convex or non-convex kites.

Vertices are the union of Voronoi and Delaunay vertices.
Edges are the intervals connecting the centers of Voronoi cells with their vertices or alternatively the centers of Delaunay cells with their vertices.
Faces are embedded quads with orthogonal diagonals and the diagonal which is a Delaunay-edge is bisected into two equal intervals by the line through the orthogonal Voronoi-edge.

Theorem 4.1. *Given a set of distinct points* $V = \{P_1, \ldots, P_n\} \in \mathbb{R}^2$ *there exists a unique Voronoi and Delaunay tessellation.*
These tessellations are dual to each other: The Delaunay vertices V *are the generating points of the Voronoi tessellation. The Delaunay faces are convex circular polygons centered at Voronoi vertices. The corresponding edges of the Voronoi and Delaunay tessellations are orthogonal.*

4.1.2 Delaunay tessellations in terms of the empty disk property

How to define Delaunay tessellations without referring to Voronoi?
We noticed that:

All faces of a Delaunay tessellation are convex circular polygons.
The corresponding Delaunay open disks D_Q contain no vertices.

and call this the *empty disk property.*

Definition 4.1. A tessellation of a planar domain is called *Delaunay* if it possesses the empty disk property.
An edge of a tessellation is called *Delaunay edge* if two faces sharing this edge do not have any of their vertices in the interior of their disks.

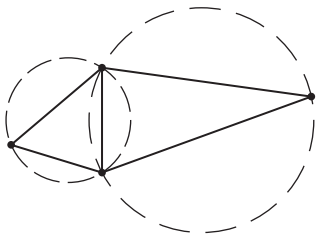

Figure 4.4. Empty disk property of Delaunay tessellations.

Theorem 4.2. *The property of being a Delaunay tessellation is invariant under Möbius transformations.*

Proof. Follows directly from the empty disk property being Möbius invariant. □

Remark 4.2. Delaunay tessellations on $\mathbb{S}^2$ can be obtained by stereographic projection.

Lemma 4.3 (angle criterion for circular quadrilaterals)**.** *Let $P_1, P_2, P_3, P_4 \in \mathbb{R}^2$ be four points in the plane cyclically ordered. Let C be the circle through P_1, P_2, P_3,*

$$\alpha \coloneqq \measuredangle P_1P_2P_3, \quad \beta \coloneqq \measuredangle P_3P_4P_1.$$

Then

$$\begin{aligned} P_4 \text{ lies outside } C &\Leftrightarrow \alpha + \beta < \pi \\ P_4 \text{ lies on } C &\Leftrightarrow \alpha + \beta = \pi \\ P_4 \text{ lies inside } C &\Leftrightarrow \alpha + \beta > \pi. \end{aligned}$$

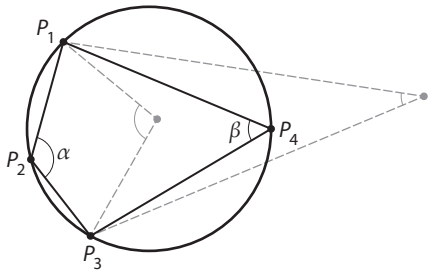

Figure 4.5. Angle criterion for circular quadrilaterals.

Proposition 4.4 (angle criterion for Delaunay triangulations)**.** *A triangulation of the plane is Delaunay if and only if for each edge the sum of the two angles opposite to this edge is less than or equal to π.*

4.2 Delaunay tessellations of piecewise flat surfaces

4.2.1 Delaunay tessellations from Voronoi tessellations

Let (M, d) be a piecewise flat surface. Let $V = \{P_1, \ldots, P_n\}$ be points on M such that $V \supset \{\text{conical singularities of } (M, d)\}$.
On M –in contrast to the planar case– it can happen that the distance between two points is realized by more than one geodesic. The suitable generalization of counting points of equal shortest distance to V is counting geodesics that realize this distance. For $P \in M$ we define

$$\Gamma_{P,V} \coloneqq \{\gamma : [0,1] \to M \text{ geodesic} \mid \gamma(0) = P,\ \gamma(1) \in V,\ \mathrm{L}(\gamma) = d(P,V)\}.$$

The 2-cells of the *Voronoi tessellation* of M with vertex set V are the connected components of

$$\{P \in M \mid \#\Gamma_{P,V} = 1\},$$

the 1-cells are the connected components of

$$\{P \in M \mid \#\Gamma_{P,V} = 2\},$$

and the 0-cells are the points in

$$\{P \in M \mid \#\Gamma_{P,V} \geqslant 3\}.$$

We can try to describe the cells in a similar manner as in the planar case. E.g. for $P' \in M$ with $\#\Gamma_{P',V} = 2$, $\gamma_1, \gamma_2 \in \Gamma_{P'}$, $\gamma_1 \neq \gamma_2$, $P_i = \gamma_1(1), P_j = \gamma_2(1) \in V$ (possibly $i = j$) the corresponding 1-cell is given by

$$\left\{P \in M \mid d(P, P_i) = d(P, P_j) < d(P, P_k)\ \forall k \neq i, j \text{ (and } \#\Gamma_{P,\{P_i,P_j\}} = 2)\right\}.$$

Example 4.1 (Voronoi tessellation of a cube)**.** Let V be the set of vertices of a cube.

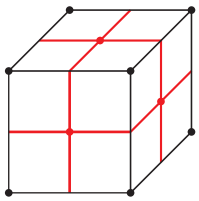

Figure 4.6. Voronoi tessellation of a cube.

Let P be an internal point of a Voronoi edge. Then there is $P_i, P_j \in V$ (possibly $i = j$) such that

$$d(P, P_i) = d(P, P_j) < d(P, P_k)\ \forall k \neq i, j.$$

This describes an *empty immersed disk* centered at P with exactly two elements of V on the boundary.[13]
The endpoints of Voronoi edges are Voronoi vertices. Let Q be such a point. Then there is $P_i, P_j, P_k \in V$ such that

$$d(Q, P_i) = d(Q, P_j) = d(Q, P_k) \leqslant d(Q, P_l)\ \forall l.$$

This describes an empty immersed disk centered at Q with at least three elements of V on the boundary.[14]
As in the plane the Delaunay tessellation is defined as dual to the Voronoi tessellation.

[13] Or one element but two different geodesics minimizing the distance to P.
[14] Or less but with at least three different geodesics minimizing the distance to P.

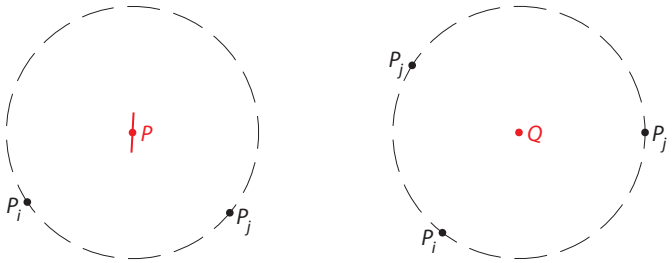

Figure 4.7. (left) An internal point P of a Voronoi edge. (right) A Voronoi vertex Q. Both are the center of an empty immersed disk on M with vertices on the boundary. The Delaunay edges are geodesic arcs connecting the points of V on the boundary, i.e. the Delaunay faces are flat circular polygons.

Remark 4.3. A *geodesic tessellation* of a piecewise flat surface (M, d) is a tessellation with flat polygonal 2-cells (compare Definition 2.6).
Delaunay tessellations are geodesic tessellations on M. The edges of Voronoi tessellations are geodesic arcs but it is not a geodesic tessellation since the faces are not flat.

Theorem 4.5. *Let (M, d) be a piecewise flat surface without boundary, $V \subset M$ a finite set of points that contains all conical singularities.*
Then there exists a unique Delaunay tessellation of M with vertex set V.

Remark 4.4.

- The proof via construction of the Voronoi tessellation can be found in [MS91].
- If one triangulates all Delaunay faces by triangulating the corresponding circular polygons in the corresponding empty immersed disks one can obtain *Delaunay triangulations*.[15]
  On the contrary, the unique Delaunay tessellation can be recovered from any Delaunay triangulation by deleting edges.
- We will show later how to construct a Delaunay triangulation starting from an arbitrary triangulation by applying an algorithm of consecutive edge flips.

4.2.2 Delaunay tessellations in terms of the empty disk property

We define Delaunay tessellations on a piecewise flat surface in a selfcontained way without referring to Voronoi.

Definition 4.2 (empty immersed disk)**.** Let (M, d) be a piecewise flat surface without boundary, $V \subset M$ a finite set of points that contains all conical singularities.
Then an *immersed empty disk* is a continuous map $\varphi : \bar{D} \to M$ such that $\varphi|_D$ is an isometric immersion[16] and $\varphi(D) \cap V = \varnothing$.

[15] In contrast to the Delaunay tessellation the Delaunay triangulation is not unique as soon as one has circular polygons which are not triangles.

[16] An isometric immersion is a local isometry, i.e. each $P \in D$ has a neighborhood which is mapped to M isometrically.

Definition 4.3 (Delaunay tessellation)**.** Let (M, d) be a piecewise flat surface without boundary, $V \subset M$ a finite set of points that contains all conical singularities.
The *Delaunay tessellation* of M with vertex set V is a cell-decomposition with the following cells:
$C \subset M$ is a closed cell of the Delaunay tessellation if there exists an immersed empty disk $\varphi : \bar{D} \to M$ such that $\varphi^{-1}(V) \neq \varnothing$ and $C = \varphi(\text{conv}\varphi^{-1}(V))$.
The cell is a 0-, 1-, 2-cell if $\varphi^{-1}(V)$ contains 1, 2, or more points respectively.

Claim 4.6. *This is indeed a tessellation.*

Remark 4.5. For the proof see [BS07].

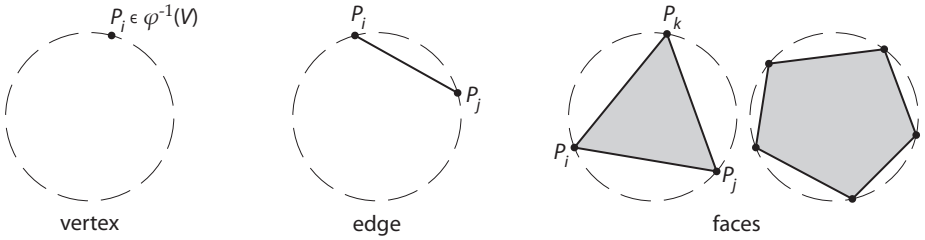

Figure 4.8. Delaunay cells and their corresponding empty immersed disks.

We characterize Delaunay triangulations in terms of a local edge property.

Definition 4.4 (Delaunay edge)**.** Let T be a geodesic triangulation of a piecewise flat surface (M, d). Let e be an interior edge of T. We can isometrically unfold the two triangles of T that are adjacent to e. e is called a *Delaunay edge* if the vertices of these unfolded triangles are not contained inside the circumcircles of the triangles.

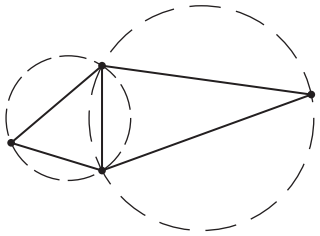

Figure 4.9. Unfolded triangles adjacent to a Delaunay edge. The inside of the circumcircles contain no vertices.

Theorem 4.7 (Characterization of Delaunay triangulations in terms of Delaunay edges)**.** *Let (M, d) be a piecewise flat surface without boundary, $V \subset M$ a finite set of points that contains all conical singularities.*
A geodesic triangulation $T \in \mathcal{T}_{M,V}$ of (M, d) is Delaunay if and only if all of its edges are Delaunay edges.

Remark 4.6. We first explain the general scheme used in the proof to obtain a locally isometric model in the Euclidean plane for parts of our surface M. We do some notably identifications on the way.

- For any face $\Delta \in F(T)$ there is a triangle in the Euclidean plane which can be isometrically immersed into the piecewise flat surface M (continuous on the boundary) such that its image corresponds to the face.
  Notationally we identify the combinatorial/metrical face on M and the unfolded Euclidean triangle.
- We extend the isometric immersion such that it stays an isometric immersion in the interior and continuous on the boundary.
  E.g. by some circular piece or a neighboring triangle.
- Note that we might not be able to extend it to the circumcircle of the unfolded triangle in the plane.
  That is why it is not obvious whether Delaunay edges imply the existence of empty immersed disks for their adjacent faces.
- Only inside the domain of this extended immersion can we be sure to draw straight lines and obtain geodesics on M and measure lengths and angles as they are on M, i.e. measure quantities in our planar isometric model that are well-defined by the piecewise flat surface.

Proof. If T is Delaunay obviously all edges are Delaunay edges.
Assume that all edges are Delaunay but the triangulation is not.

Any face $\Delta \in F(T)$ can be isometrically unfolded into the plane. We denote its circumcircle in the plane by D_Δ.
For an edge a of Δ consider the one-parameter family of circles in the plane through its endpoints. a divides the corresponding open disks into two parts of which we take the one that does not intersect Δ. We call them disk segments which fit to Δ along a.

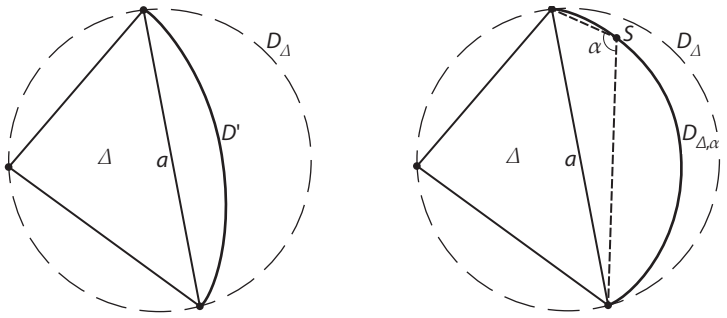

Figure 4.10. (left) Unfolded face Δ with circumcircle D_Δ and disk segment D' fitting to Δ along a. (right) We extend the isometric immersion of Δ behind the edge a to the largest possible disk segment $D_{\Delta,a}$. To every $(\Delta, a, S) \in \mathcal{A}$ we associate an angle α.

$$\mathcal{D}_{\Delta,a} \coloneqq \{D' \mid \text{disk segment fitting to } \Delta \text{ along } a,\\ \text{the isometric immersion of } \Delta \text{ can be extended to } D'\\ \text{(continuously to } \bar{D}'),\\ D' \cap V = \varnothing\}$$

For any edge a of a face Δ we denote the largest such disk segment by

$$D_{\Delta,a} \coloneqq \bigcup_{D' \in \mathcal{D}_{\Delta,a}} D'.$$

If $\mathcal{D}_{\Delta,a}$ is bounded, then $D_{\Delta,a} \in \mathcal{D}_{\Delta,a}$ and there has to be a vertex on the circular arc bounding $D_{\Delta,a}$, i.e.

$$(\partial D_{\Delta,a} \backslash \bar{a}) \cap V \neq \varnothing.$$

Otherwise we could enlarge $D_{\Delta,a}$.

A face Δ which has no empty immersed disk must have an edge a such that $(\bar{D}_{\Delta,a} \backslash \bar{a}) \subset D_\Delta$. Thus the set

$$\mathcal{A} \coloneqq \{(\Delta, a, S) \in F \times E \times V \mid \Delta \text{ has no empty immersed disk},\\ a \text{ is edge of } \Delta \text{ with } (\bar{D}_{\Delta,a} \backslash \bar{a}) \subset D_\Delta,\\ S \in (\partial D_{\Delta,a} \backslash \bar{a}) \cap V\}$$

is not empty.

We introduce the angle $\alpha : \mathcal{A} \to (0, \pi)$,

$$\alpha\,(\Delta, (BC), S) \coloneqq \measuredangle BSC.$$

Let $(\Delta, a, S) \in \mathcal{D}$ such that

$$\alpha(\Delta, a, S) = \max_{(\tilde{\Delta}, \tilde{a}, \tilde{S}) \in \mathcal{A}} \alpha(\tilde{\Delta}, \tilde{a}, \tilde{S}). \tag{4.1}$$

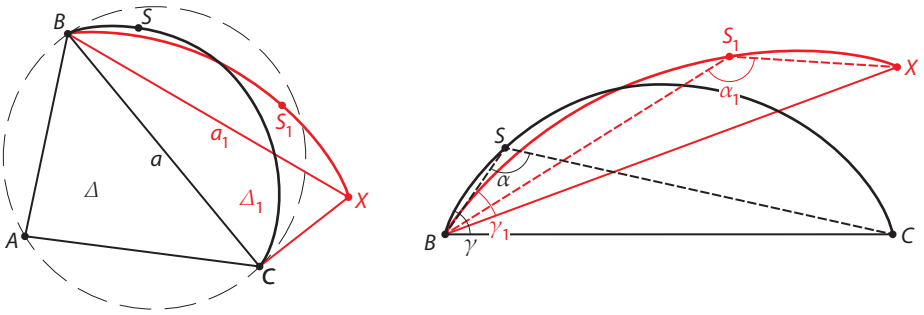

Figure 4.11. (left) For $(\Delta, a, S) \in \mathcal{A}$ we obtain a neighboring element $(\Delta_1, a_1, S_1 \in \mathcal{A}$. (right) We find $\alpha(\Delta_1, a_1, S_1) > \alpha(\Delta, a, S)$ since $\gamma_1 < \gamma$ in contradiction to the assumption.

Let Δ_1 be the face sharing the edge a with Δ. We can isometrically unfold it to the same plane as Δ. Let B, C be the endpoints of a and X the opposite vertex of Δ_1.

$$a \text{ Delaunay edge } \Rightarrow X \notin D_\Delta.$$

Since no triangle may contain any vertices we also have $S \notin \Delta_1$.
Let a_1 be the edge of Δ_1 closest to S, say $a_1 = (BX)$. Then there is $S_1 \in V$ (possibly $S_1 = S$) such that

$$(\Delta_1, a_1, S_1) \in \mathcal{A}.$$

Let us denote the corresponding angles by $\alpha \coloneqq \alpha(\Delta, a, S)$ and $\alpha_1 \coloneqq \alpha(\Delta_1, a_1, S_1)$. Due to Lemma 4.8 the angle $\gamma \coloneqq \pi - \alpha$ is the intersection angle of the circular arc of $\partial D_{\Delta,a}$ with a at B. Similarly γ_1.
Clearly, $\gamma > \gamma_1$ which implies

$$\alpha < \alpha_1$$

in contradiction to (4.1). □

Lemma 4.8. *Let B, S, C be three points on a circle, $\alpha \coloneqq \sphericalangle BSC$. Then the intersection angle between the tangent to the circle at B and the secant (BC) as depicted in Figure 4.12 is equal to α.*

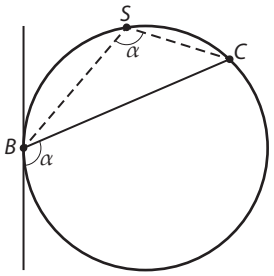

Figure 4.12. Angle in a circular arc.

Proof. While moving S along the circular arc the angle $\alpha = \sphericalangle BSC$ stays constant. In the limit $S \to B$ the edge (BS) becomes the tangent at B and $(SC) \to (BC)$. □

The characterization of Delaunay triangulations in terms of Delaunay edges allows us to formulate an angle criterion as in the planar case.

Proposition 4.9 (Angle criterion for Delaunay triangulations)**.** *A geodesic triangulation of a piecewise flat surface is Delaunay if and only if for every edge the sum of the two angles opposite to this edge is less than or equal to π.*

This is a practical geometric characterization since angles can be measured directly on the piecewise flat surface without any need to find empty immersed disks. Recalling (3.12) we notice at this point

Proposition 4.10. *The discrete cotan Laplace operator of a geodesic triangulation T of a piecewise flat surface (M, d) has non-negative weights if and only if T is Delaunay.*

4.3 The edge-flip algorithm

Let T be a geodesic triangulation of a piecewise flat surface (M, d).
If we unfold two adjacent triangles of T into the plane, we obtain a quadrilateral Q, where one of its diagonals e corresponds to the shared edge of the triangles and the other one e^* corresponds to the edge resulting in an edge flip of e if possible.

Lemma 4.11. *Every non-Delaunay edge of T can be flipped and the flipped edge is then Delaunay.*

Proof. Let e be a non-Delaunay edge.
We use Lemma 2.8 to characterize whether e can be flipped. The sum of the angles opposite to e in the adjacent triangles is greater than π. Therefore the two triangles have to be different since the sum of all angles in a triangle is equal to π. The two triangles form a convex quadrilateral as can be seen e.g. from Figure 4.5. So e can be flipped and the sum of the angles opposite to the flipped edge e^* is less than or equal to π. □

The following question emerges.

> Can any given triangulation be made Delaunay by consecutive edge-flips?

Definition 4.5. We denote the set of all geodesic triangulations of a given piecewise flat surface (M, d) with vertex set V by $\mathcal{T}_{M,V}$.

The edge-flip algorithm acts on $\mathcal{T}_{M,V}$ in the following way.

Data: Some $T \in \mathcal{T}_{M,V}$.
Result: A Delaunay triangulation $T \in \mathcal{T}_{M,V}$.
while T *is not Delaunay* **do**
  Take any non-Delaunay edge e of T;
  Flip e in T;
end

Figure 4.13. Edge-flip algorithm.

Example 4.2. We make the triangulation of the tetrahedron shown in Figure 4.14 Delaunay by applying the edge-flip algorithm.

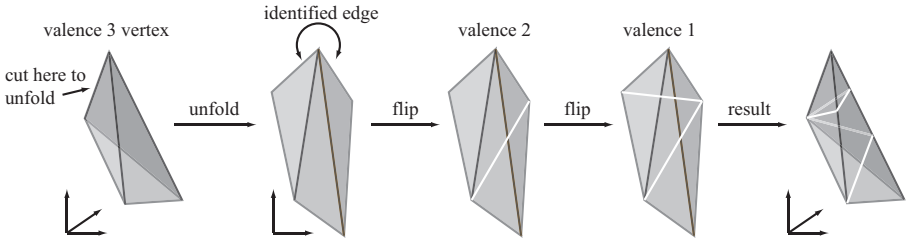

Figure 4.14. Making a given triangulation Delaunay.

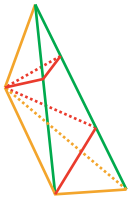

Figure 4.15. Result with colored edges. Green and yellow edges are original edges. Red and yellow edges are Delaunay edges.

Note that the resulting triangulation is not regular and has a vertex of valence one.

Theorem 4.12. *The edge-flip algorithm terminates for any start triangulation $T \in \mathcal{T}_{M,V}$ after a finite number of steps.*

Remark 4.7. Removing all edges which would stay Delaunay upon an edge-flip we obtain the unique Delaunay tessellation. Claiming the existence of some geodesic triangulation on any piecewise flat surface this implies Theorem 4.5. In practice having some start triangulation is not an issue since the standard ways of prescribing a piecewise flat surface already includes a triangulation.

The state of the algorithm is determined by the current triangulation in $\mathcal{T}_{M,V}$. We address the question of possible loops in the algorithm later by means of a function $f : \mathcal{T}_{M,V} \to \mathbb{R}$ that decreases on each step.

For a piecewise flat surface –in contrast to triangulations of a finite set of points in the plane– the set of all triangulations $\mathcal{T}_{M,V}$ is an infinite set in general.

Example 4.3 (infinitely many triangulations of the cube with arbitrary long edges)**.** Consider a standard cube with vertex set V. Unwrapping the cube as in Figure 2.8 suggests how to create an arbitrary long edge between two vertices of V. Completing to a triangulation we conclude that there are infinitely many triangulations of the cube.

So even with the exclusion of loops the algorithm might not terminate.

Definition 4.6 (proper function)**.** We call a function $f : \mathcal{T}_{M,V} \to \mathbb{R}$ proper if for each $c \in \mathbb{R}$ the sublevel set $\{T \in \mathcal{T}_{M,V} \mid f(T) \leqslant c\}$ is finite.

Having a proper decreasing function we can ensure termination after a finite number of steps.

Example 4.4 (edge length function)**.** For an edge e of a triangulation T we denote its length by $l(e)$. Consider the function $l : \mathcal{T}_{M,V} \to \mathbb{R}$ which assigns to each triangulation its maximal edge length

$$l(T) \coloneqq \max_{e \in E(T)} l(e).$$

As we have seen in Example 4.3 the function l might be unbound on $\mathcal{T}_{M,V}$. Nonetheless bounding l only leaves a finite number of triangulations.

Claim 4.13. *The edge length function l is proper.*

4.3.1 Dirichlet energy and edge-flips

Let T be a geodesic triangulation of a piecewise flat surface (M, d). We investigate the local change in the Dirichlet energy of a discrete function $u : V(T) \to \mathbb{R}$ upon an edge-flip.

The geometry of a convex non-degenerate quadrilateral Q with vertices $1, 2, 3, 4$ denoted in counter-clockwise direction is completely determined by the values of $r_1, r_2, r_3, r_4 > 0$ and $\theta \in (0, \pi)$ as depicted in Figure 4.16. We denote such a quadrilateral by $Q(r_1, r_2, r_3, r_4, \theta)$.

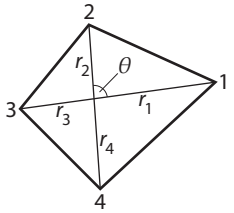

Figure 4.16. A convex non-degenerate quadrilateral $Q(r_1, r_2, r_3, r_4, \theta)$.

Lemma 4.14 (Rippa's Lemma)**.** *Let u_1, u_2, u_3, u_4 be the values of a function on the vertices of the convex non-degenerate quadrilateral $Q(r_1, r_2, r_3, r_4, \theta)$. Let $u_{13} : Q \to \mathbb{R}$ and be the linear interpolation which is affine on the triangles* (123) *and* (134) *whereas $u_{24} : Q \to \mathbb{R}$ is the linear interpolation affine on* (234) *and* (241)*. Let u_0 and u_0^* be the values at the intersection point of the diagonals of u_{13} and u_{24} respectively.*
Then the difference of the corresponding Dirichlet energies is

$$E(u_{13}) - E(u_{24}) = \frac{1}{4} \frac{(u_0 - u_0^*)^2}{\sin\theta} \frac{(r_1 + r_3)(r_2 + r_4)}{r_1 r_2 r_3 r_4} (r_1 r_3 - r_2 r_4). \tag{4.2}$$

Proof. The diagonals of Q separate the quadrilateral into four triangles Δ_1, Δ_2, Δ_3, Δ_4. Both linear interpolations are affine on each of these triangles while the Dirichlet energy of any affine function $u : \Delta_i \to \mathbb{R}$ on the triangle Δ_i is given by

$$E_{\Delta_i}(u) = \frac{1}{2} \int_{\Delta_i} |\nabla u|^2 \, \mathrm{d}A = \frac{1}{2}(u_x^2 + u_y^2) A(\Delta_i).$$

Consider the triangle Δ_1. The interpolation $u \coloneqq u_{13}$ is determined by the values u_0, u_1, u_2 and the geometric data r_1, r_2, θ of the triangle. Choosing a coordinate system such that the x-axis is aligned with the edge r_1 of Δ_1

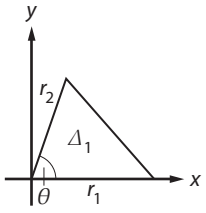

Figure 4.17. Triangle Δ_1 in suitable coordinate system.

we find

$$\begin{aligned} u_1 - u_0 &= u_x r_1 \\ u_2 - u_0 &= u_x r_2 \cos\theta + u_y r_2 \sin\theta, \end{aligned}$$

from which we obtain the partial derivatives u_x and u_y of u on Δ_1

$$\begin{aligned} u_x &= \frac{u_1 - u_0}{r_1} \\ u_y &= \frac{1}{\sin\theta}\left(\frac{u_2 - u_0}{r_2} - \frac{u_1 - u_0}{r_1}\cos\theta\right). \end{aligned}$$

For the gradient we get

$$|\nabla u|^2 = u_x^2 + u_y^2 = \frac{1}{\sin^2\theta}\left(\left(\frac{u_1 - u_0}{r_1}\right)^2 + \left(\frac{u_2 - u_0}{r_2}\right)^2 - 2\frac{(u_1 - u_0)(u_2 - u_0)\cos\theta}{r_1 r_2}\right).$$

The gradient of the interpolation $u^* \coloneqq u_{24}$ on Δ_1 is obtained by replacing u_0 by u_0^*. With $A(\Delta_1) = \frac{1}{2} r_1 r_2 \sin\theta$ the difference of the Dirichlet energies on Δ_1 is

$$\begin{aligned} E_{\Delta_1}(u) - E_{\Delta_1}(u^*) &= \frac{1}{2}\Big(|\nabla u|^2 - |\nabla u^*|^2\Big) A(\Delta_1) \\ &= \frac{r_1 r_2}{4\sin\theta}\Bigg((u_0^2 - u_0^{*2})\left(\frac{1}{r_1^2} + \frac{1}{r_2^2} - \frac{2\cos\theta}{r_1 r_2}\right) \\ &\quad + 2(u_0 - u_0^*)\left(-\frac{u_1}{r_1^2} - \frac{u_2}{r_2^2} + \frac{(u_1 + u_2)\cos\theta}{r_1 r_2}\right)\Bigg) \\ &= \frac{u_0 - u_0^*}{4\sin\theta}\Bigg((u_0 + u_0^*)\left(\frac{r_2}{r_1} + \frac{r_1}{r_2} - 2\cos\theta\right) \\ &\quad + 2\left(-u_1\frac{r_2}{r_1} - u_2\frac{r_1}{r_2} + (u_1 + u_2)\cos\theta\right)\Bigg). \end{aligned}$$

For the difference on Δ_2 we replace $r_1 \to r_2$, $r_2 \to r_3$, $\theta \to \pi - \theta$ and obtain

$$\begin{aligned} E_{\Delta_2}(u) - E_{\Delta_2}(u^*) = \frac{u_0 - u_0^*}{4\sin\theta}\Bigg((u_0 + u_0^*)\left(\frac{r_3}{r_2} + \frac{r_2}{r_3} + 2\cos\theta\right) \\ + 2\left(-u_2\frac{r_3}{r_2} - u_3\frac{r_2}{r_3} - (u_2 + u_3)\cos\theta\right)\Bigg). \end{aligned}$$

Similarly for Δ_3 and Δ_4.

We sum up over all four triangles obtaining the difference of the Dirichlet energies on the whole quadrilateral

$$\begin{aligned}
E(u) - E(u^*) &= \sum_{i=1}^{4} \Big(E_{\Delta_i}(u) - E_{\Delta_i}(u^*) \Big) \\
&= \frac{u_0 - u_0^*}{4 \sin\theta} \Bigg((u_0 + u_0^*) \Big(\frac{r_1}{r_2} + \frac{r_2}{r_3} + \frac{r_3}{r_4} + \frac{r_4}{r_1} + \frac{r_2}{r_1} + \frac{r_3}{r_2} + \frac{r_4}{r_3} + \frac{r_1}{r_4} \Big) \\
&\quad - 2 \Big(u_1 \Big(\frac{r_2}{r_1} + \frac{r_4}{r_1} \Big) + u_2 \Big(\frac{r_3}{r_2} + \frac{r_1}{r_2} \Big) + u_3 \Big(\frac{r_4}{r_3} + \frac{r_2}{r_3} \Big) + u_4 \Big(\frac{r_1}{r_4} + \frac{r_3}{r_4} \Big) \Big) \Bigg) \\
&= \frac{u_0 - u_0^*}{4 \sin\theta} \Bigg((u_0 + u_0^*) \Big((r_2 + r_4) \Big(\frac{1}{r_1} + \frac{1}{r_3} \Big) + (r_1 + r_3) \Big(\frac{1}{r_2} + \frac{1}{r_4} \Big) \Big) \\
&\quad - 2 \Big((r_2 + r_4) \Big(\frac{u_1}{r_1} + \frac{u_3}{r_3} \Big) \Big) + (r_1 + r_3) \Big(\frac{u_2}{r_2} + \frac{u_4}{r_4} \Big) \Big) \Bigg).
\end{aligned}$$

The values u_0 and u_0^* come from the different linear interpolations along the diagonals (13) and (24) respectively.

$$\begin{aligned}
u_0 &= \frac{r_3 u_1 + r_1 u_3}{r_1 + r_3} \\
u_0^* &= \frac{r_4 u_2 + r_2 u_4}{r_2 + r_4}
\end{aligned}$$

Using

$$\begin{aligned}
\frac{u_1}{r_1} + \frac{u_3}{r_3} &= u_0 \frac{r_1 + r_3}{r_1 r_3} \\
\frac{u_2}{r_2} + \frac{u_4}{r_4} &= u_0 \frac{r_2 + r_4}{r_2 r_4}
\end{aligned}$$

we can eliminate all dependence of the vertex values from the difference of the Dirichlet energies

$$\begin{aligned}
E(u) - E(u^*) &= \frac{u_0 - u_0^*}{4 \sin\theta} (r_1 + r_3)(r_2 + r_4) \left((u_0 + u_0^*) \left(\frac{1}{r_1 r_3} + \frac{1}{r_2 r_4} \right) - 2 \left(\frac{u_0}{r_1 r_3} + \frac{u_0^*}{r_2 r_4} \right) \right) \\
&= \frac{u_0 - u_0^*}{4 \sin\theta} (r_1 + r_3)(r_2 + r_4) \left(u_0 \left(\frac{1}{r_2 r_4} - \frac{1}{r_1 r_3} \right) + u_0^* \left(\frac{1}{r_1 r_3} - \frac{1}{r_2 r_4} \right) \right) \\
&= \frac{(u_0 - u_0^*)^2}{4 \sin\theta} (r_1 + r_3)(r_2 + r_4) \frac{r_1 r_3 - r_2 r_4}{r_1 r_2 r_3 r_4}.
\end{aligned}$$

□

We notice that all factors in (4.2) but the last are positive.[17] The sign of the last factor determines which edge is Delaunay.

[17] Note that for $u_0 - u_0^* \neq 0$ we require that not all of u_1, u_2, u_3, u_4 are equal.

Lemma 4.15 (circular quadrilaterals)**.** *The quadrilateral $Q(r_1, r_2, r_3, r_4, \theta)$ is circular if and only if $r_1 r_3 = r_2 r_4$.*
Furthermore

$$r_1 r_3 > r_2 r_4 \Leftrightarrow (24) \text{ Delaunay}$$
$$r_1 r_3 < r_2 r_4 \Leftrightarrow (13) \text{ Delaunay.}$$

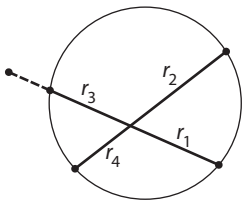

Figure 4.18. Circularity criterion for a convex quadrilateral in terms of lengths of diagonal segments.

Corollary 4.16. *Suppose that not all of the vertex values u_1, u_2, u_3, u_4 are equal. Then*

$$E(u_{13}) = E(u_{24}) \Leftrightarrow Q \text{ circular, i.e. both edges are Delaunay}$$
$$E(u_{13}) > E(u_{24}) \Leftrightarrow (24) \text{ Delaunay}$$
$$E(u_{13}) < E(u_{24}) \Leftrightarrow (13) \text{ Delaunay.}$$

So an edge-flip from a non-Delaunay edge to a Delaunay edge decreases the Dirichlet energy.

Remark 4.8. Note that the Dirichlet energy depends on the triangulation T as well as on the function $u : V(T) \to \mathbb{R}$. To ensure that the Dirichlet energy decreases upon an edge-flip u is required to be non-constant close to the edge.

4.3.2 Harmonic index

We introduce a related function that decreases on each step of the edge-flip algorithm and only depends on the triangulation.

Definition 4.7 (harmonic index)**.** For a triangle Δ with side-lengths a, b, c we define its *harmonic index* to be

$$h(\Delta) \coloneqq \frac{a^2 + b^2 + c^2}{A(\Delta)},$$

and for a geodesic triangulation $T \in \mathcal{T}_{M,V}$ of a piecewise flat surface

$$h(T) \coloneqq \sum_{\Delta \in F(T)} h(\Delta).$$

Lemma 4.17. *Let Δ be a triangle with angles α, β, γ. Then*

$$h(\Delta) = 4(\cot\alpha + \cot\beta + \cot\gamma).$$

Proof. Denote by a, b, c the lengths of the sides of Δ opposite α, β, γ respectively. Consider the height h_a on a.

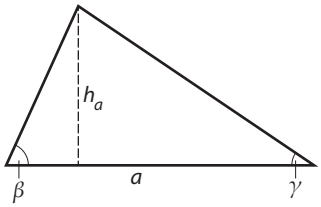

Figure 4.19. Triangle with side lengths a, b, c, corresponding heights h_a, h_b, h_c and angles α, β, γ.

Then

$$a = h_a(\cot\beta + \cot\gamma),$$

and therefore

$$a^2 = 2A(\Delta)(\cot\beta + \cot\gamma).$$

Adding this up with the corresponding formulas for the remaining edge lengths we obtain

$$a^2 + b^2 + c^2 = 4A(\Delta)(\cot\alpha + \cot\beta + \cot\gamma).$$

□

What has the harmonic index of a triangulation T to do with the Dirichlet energy?

Lemma 4.18. *Let T be a geodesic triangulation of a piecewise flat surface, $\varphi_i : V(T) \to \mathbb{R}$, $\varphi_i(j) \coloneqq \delta_{ij}$ the basis functions on T. Then*

$$h(T) = 8 \sum_{i \in V(T)} E(\varphi_i).$$

Proof. The Dirichlet energy of φ_i is given by

$$E(\varphi_i) = \frac{1}{4} \sum_{j \in V : (ij) \in E} (\cot\alpha_{ij} + \cot\alpha_{ji}).$$

Summing along all vertices $i \in V$ amounts in counting every angle twice

$$\sum_{i \in V} E(\varphi_i) = \frac{1}{2} \sum_{(ij) \in E} (\cot\alpha_{ij} + \cot\alpha_{ji}).$$

□

Corollary 4.19. *The harmonic index decreases on each step of the edge-flip algorithm.*

Lemma 4.20. *The harmonic index $h : \mathcal{T}_{M,V} \to \mathbb{R}$ is a proper function.*

Proof. Denote by A the total area of the surface M. We do a very coarse estimation using the maximal edge length $l : \mathcal{T}_{M,V} \to \mathbb{R}$ introduced in Example 4.4:

$$h(T) = \sum_{\Delta \in F(T)} h(\Delta) \geqslant \frac{l(T)}{A}.$$

So for $c \in \mathbb{R}$

$$h(T) \leqslant c \;\Rightarrow\; l(T) \leqslant \sqrt{h(T)A} = \sqrt{cA},$$

and we know that l is proper. □

We conclude that the edge-flip algorithm terminates after a finite number of steps. We have therefore proven Theorem 4.12. But even more

Theorem 4.21. *Let (M, d) be a piecewise flat surface without boundary, $V \subset M$ a finite set of points that contains all conical singularities.*
Let $f : V \to \mathbb{R}$. For each triangulation $T \in \mathcal{T}_{M,V}$ let $f_T : M \to \mathbb{R}$ be the piecewise linear interpolation of f which is affine on the faces of T.
Then the minimum of the Dirichlet energy $E(f_T) = \int_M |\nabla f_T|^2 \, \mathrm{d}A$ among all possible triangulations is attained on a Delaunay triangulation $T_D^\Delta \in \mathcal{T}_{M,V}$ of (M, d):

$$\min_{T \in \mathcal{T}_{M,V}} E(f_T) = E(f_{T_D^\Delta}).$$

4.4 Discrete Laplace-Beltrami operator

Let (M, d) be a piecewise flat surface without boundary, $V \subset M$ a finite set of points that contains all conical singularities.
Let T_D be the Delaunay tessellation of M and $T_D^\Delta \in \mathcal{T}_{M,V}$ some Delaunay triangulation of T_D. Recalling (3.12) we see that for an edge $(ij) \in E$ we have

$$\nu(ij) = 0 \;\Leftrightarrow\; \alpha_{ij} + \alpha_{ji} = \pi,$$

which is the case for circular quadrilaterals. So the edges in T_D^Δ coming from triangulating circular polygons of the Delaunay tessellation T_D have zero weights. The weights of edges on the boundary of circular polygons of T_D are independent of the chosen triangulation as can be seen in Figure 4.20.

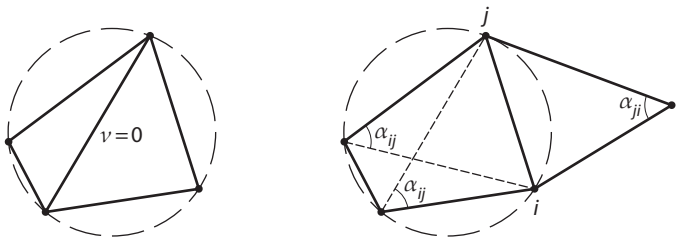

Figure 4.20. Cotan-weights of the Delaunay tessellation. (left) An edge coming from triangulating circular polygons has zero cotan-weight. (right) The cotan-weight of an edge on the boundary of a circular polygon does not depend on the triangulation.

So the cotan-weights are well-defined on the edges of the Delaunay tessellation.

Definition 4.8 (discrete Laplace-Beltrami operator)**.** Let (M, d) be a piecewise flat surface without boundary, $V \subset M$ a finite set of points that contains all conical singularities.
Let T_D be the Delaunay tessellation of M.
Then the *discrete Laplace-Beltrami operator* of (M, d) is defined by

$$\Delta f(i) = \sum_{e=(ij)\in E(T_D)} \nu(e)\,(f(i) - f(j))$$

for any function $f : V \to \mathbb{R}$.
The corresponding Dirichlet energy on (M, d) is defined by

$$E(f) \coloneqq \frac{1}{2} \sum_{e=(ij)\in E(T_D)} \nu(e)\,(f(i) - f(j))^2\,,$$

where ν are the cotan-weights as defined in (3.3) coming from any Delaunay triangulation $T_D^{\Delta} \in \mathcal{T}_{M,V}$ of T_D.

Remark 4.9.

- The sum can be taken over all edges of any Delaunay triangulation as we have seen above.
  The notion of neighboring vertices might differ from the one given by the "extrinsic triangulation" of a polyhedral surface in $\mathbb{R}^N$. Also triangles of a Delaunay triangulation are not necessarily planar in $\mathbb{R}^N$ anymore.

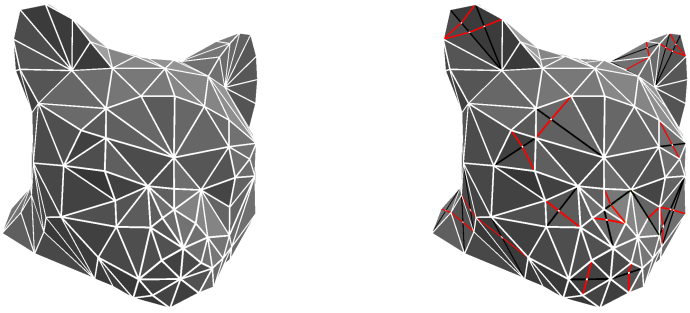

Figure 4.21. Simplicial cat. (left) Triangulation coming from the simplicial surface. (right) Delaunay triangulation (white and red edges).

- The Laplace-Beltrami operator is a well-defined property of the Delaunay tessellation T_D which is uniquely determined by (M, d) and the vertex set V. So we have defined a unique discrete Laplace-Beltrami operator of the piecewise flat surface (M, d), which is determined by the polyhedral metric only, i.e. invariant w.r.t. isometries.
- In Proposition 4.10 we have seen that all weights of the Delaunay triangulation are non-negative. With above considerations we can now conclude that all weights of the Delaunay tessellation are positive. So for the discrete Laplace-Beltrami operator we can apply the results of the theory of discrete Laplace operators with positive weights. We are assured to have the maximum principle and unique minima of the Dirichlet energy.

4.5 Simplicial minimal surfaces (II)

Having the discrete Laplace-Beltrami operator we can improve the definition of simplicial minimal surfaces of Section 3.4.

Definition 4.9 (simplicial minimal surface)**.** Let $f : \mathcal{S} \to S \subset \mathbb{R}^N$ be a simplicial surface and T its triangulation. Then

$$\begin{aligned} S \text{ minimal (in the wide sense)} &:\Leftrightarrow \Delta f = 0 \\ S \text{ minimal (in the narrow sense)} &:\Leftrightarrow \Delta f = 0 \text{ and } T \text{ is Delaunay,} \end{aligned}$$

where in both cases Δ is the discrete Laplace-Beltrami operator of S.

Remark 4.10.

- The Laplace-Beltrami operator coincides with the cotan-Laplace operator only in the narrow definition. So only in this case the surface is actually a critical point of the area functional.
- The Laplace-Beltrami operator has all positive weights. If f is harmonic the maximum principle (Proposition 3.10) implies that any vertex point $f(i)$ lies in the convex hull of its neighbors:

  $$f(i) \in \operatorname{conv}\{f(j) \in \mathbb{R}^n \mid (ij) \in E(T_D)\},$$

  where neighbors are determined by the Delaunay tessellation T_D of S.

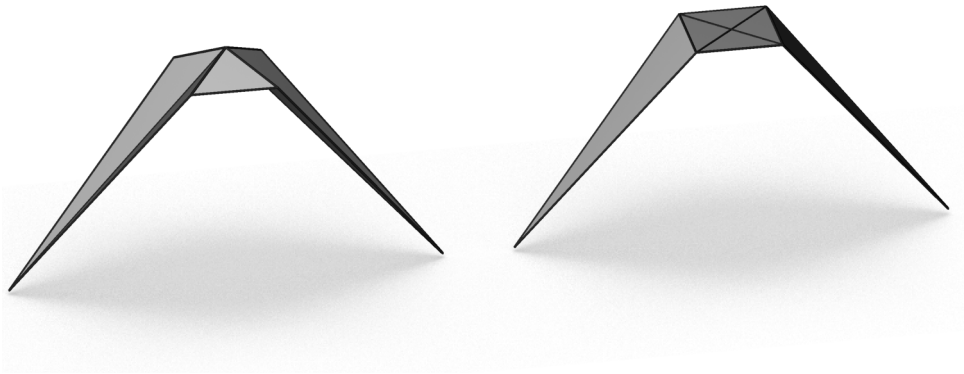

Figure 4.22. (left) Simplicial surface which is minimal with respect to the definition of Section 3.4. It violates the maximum principle. (right) Corresponding minimal surface (in the narrow sense) with respect to Definition 4.9. It satisfies the maximum principle. By "corresponding" we mean that it is obtained by applying Algorithm 4.23 to the left surface.

In the wide definition the neighbors satisfying the maximum principle might be different from the ones given by the triangulation of S, where in the narrow definition they coincide.

This new definition leads to the following algorithm producing minimal surfaces in the narrow sense, if it converges.

Data: Simplicial surface $f : \mathcal{S} \to S \subset \mathbb{R}^N$ with triangulation T.
Result: Simplicial minimal surface in the narrow sense.
while S *is not minimal in the narrow sense* **do**
  Compute Delaunay triangulation $\tilde{T}$ of S (use Algorithm 4.13);
  Compute $\tilde{f}$ such that
$$\Delta_{(S,\tilde{T})}\tilde{f} = 0,$$
  which defines a new simplicial surface $\tilde{S}$;
  Replace S by the new surface $\tilde{S}$;
  Replace T by $\tilde{T}$;
end

Figure 4.23. Simplicial minimal surface algorithm (with intrinsic discrete Laplace-Beltrami-operator and change of combinatorics).

Remark 4.11. The state of the algorithm is determined by the simplicial surface S and its triangulation T.
In each step of the while-loop we replace

$$(S, T) \leftarrow (\tilde{S}, \tilde{T}),$$

where $\tilde{T}$ is the Delaunay triangulation of S which might not be Delaunay anymore for $\tilde{S}$.
Besides using the intrinsic Laplace-Beltrami operator the fundamental difference to Algorithm 3.6 is the change of combinatorics in each step.

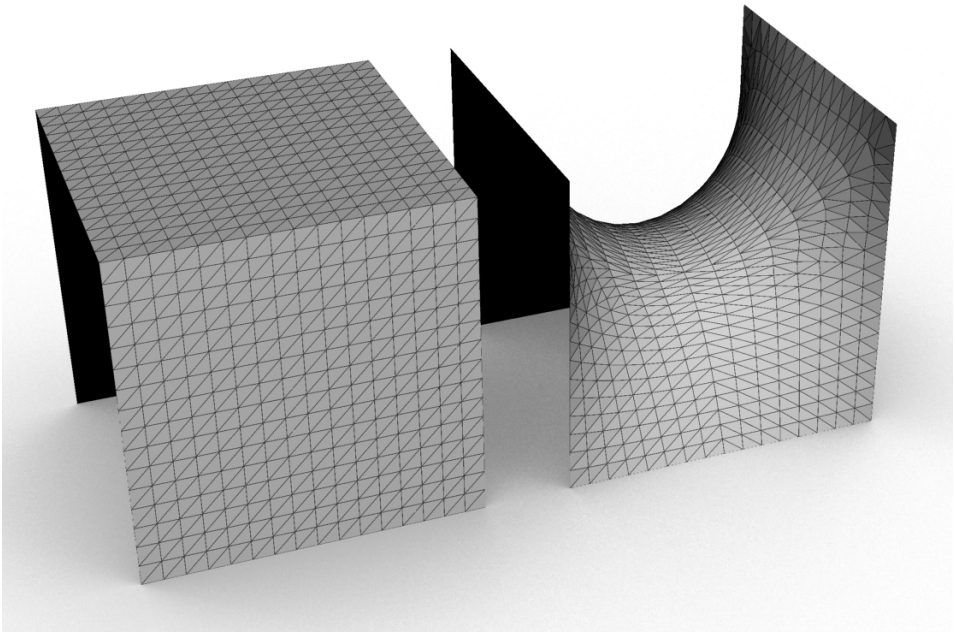

Figure 4.24. Simplicial minimal surface from Algorithm 4.23.

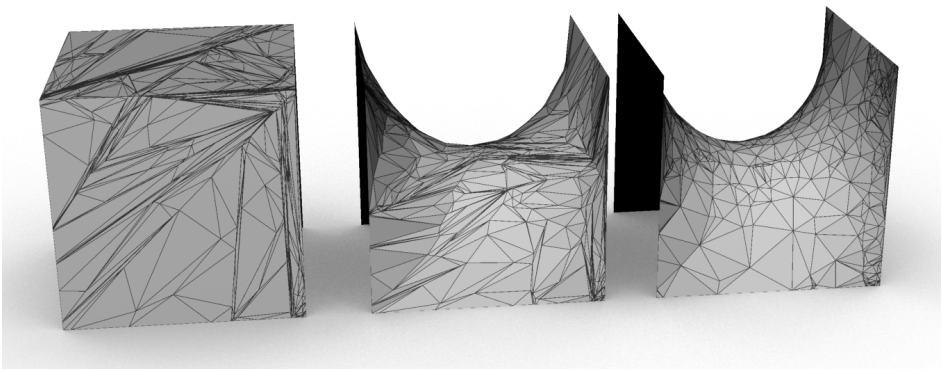

Figure 4.25. Using the intrinsic Laplace-Beltrami operator with and without change of combinatorics. Starting with a random triangulation the change becomes particularly eminent. (left) Random start triangulation. (middle) Result of Algorithm 4.23 without change of combinatorics. (right) Result of Algorithm 4.23 with change of combinatorics.

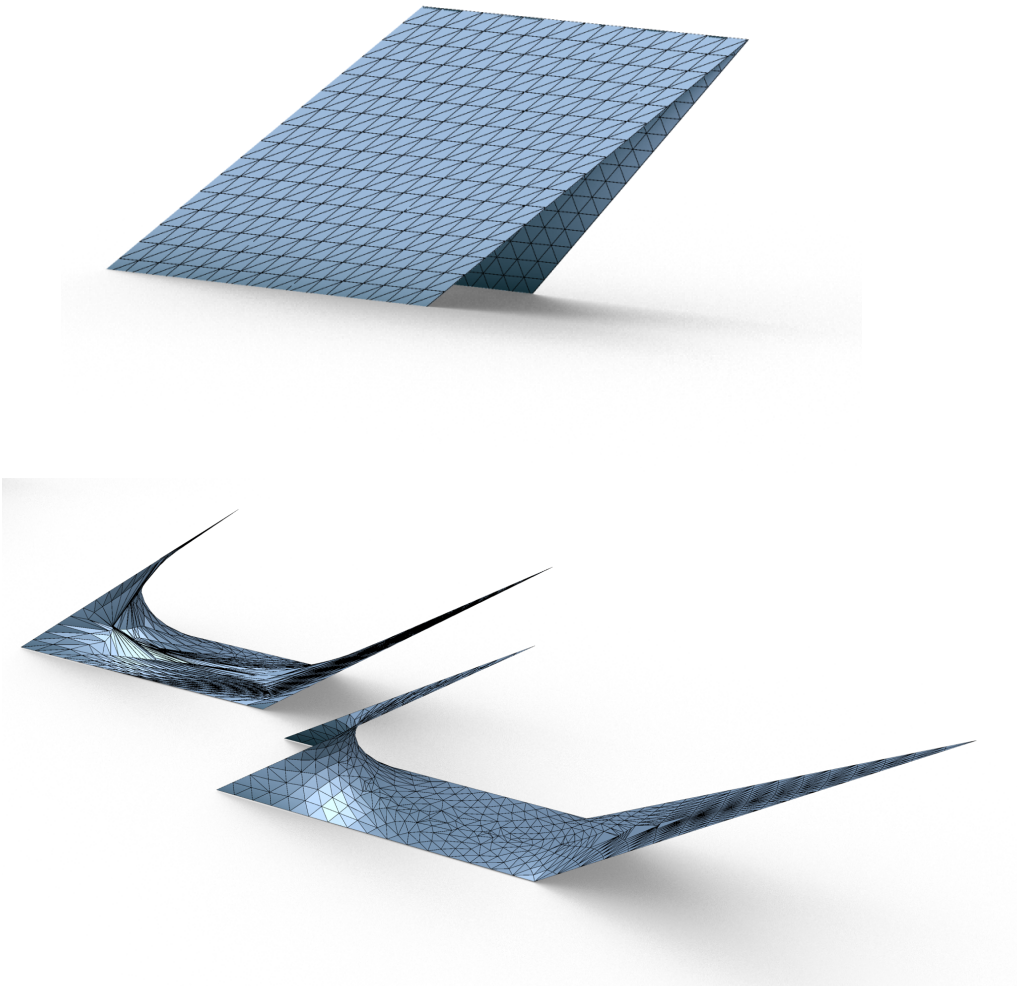

Figure 4.26. Comparing intrinsic and extrinsic Laplace-Beltrami operator. We start with a triangulation which is not suitable for the resulting minimal surface. (top) Start triangulation. (bottom left) Result of applying Algorithm 3.6 for some time. No convergence! (bottom right) Result of Algorithm 4.23.

References

[BI08] Alexander I. Bobenko and Ivan Izmestiev. "Alexandrov's theorem, weighted Delaunay triangulations, and mixed volumes". In: *Annales de l'Institut Fourier* 58.2 (2008), pp. 447–505. DOI: 10.5802/aif.2358.

[BS07] Alexander I. Bobenko and Boris A. Springborn. "A Discrete Laplace-Beltrami Operator for Simplicial Surfaces". English. In: *Discrete and Computational Geometry* 38.4 (2007), pp. 740–756. ISSN: 0179-5376. DOI: 10.1007/s00454-007-9006-1.

[FW99] George K. Francis and Jeffrey R. Weeks. "Conway's ZIP Proof". In: *The American Mathematical Monthly* 106.5 (May 1999), pp. 393–399. URL: http://www.jstor.org/stable/2589143.

[MS91] Howard Masur and John Smillie. "Hausdorff Dimension of Sets of Nonergodic Measured Foliations". In: *Annals of Mathematics* 134.3 (Nov. 1991), pp. 455–543. ISSN: 0003-486X. DOI: 10.2307/2944356.

[PP93] Ulrich Pinkall and Konrad Polthier. "Computing discrete minimal surfaces and their conjugates". In: *Experiment. Math.* 2.1 (1993), pp. 15–36. URL: http://projecteuclid.org/euclid.em/1062620735.

[Sec] Stefan Sechelmann. *Homepage*. URL: http://www.sechel.de.